sustainability

MDPI

Article

Novel Pervaporation Membranes Based on Biopolymer Sodium Alginate Modified by FeBTC for Isopropanol Dehydration

Anna Kuzminova *, Mariia Dmitrenko, Anton Mazur, Sergey Ermakov and Anastasia Penkova

St. Petersburg State University, 199034 St. Petersburg, Russia; m.dmitrienko@spbu.ru (M.D.); a.mazur@spbu.ru (A.M.); s.ermakov@spbu.ru (S.E.); a.penkova@spbu.ru (A.P.)
* Correspondence: ai.kuzminova@mail.ru; Tel.: +7-(812)-363-60-00 (ext. 3367)

Abstract: Modern society strives for the development of sustainable processes that are aimed at meeting human needs while preserving the environment. Membrane technologies satisfy all the principles of sustainability due to their advantages, such as cost-effectiveness, environmental friendliness, absence of additional reagents and ease of use compared to traditional separation methods. In the present work, novel green membranes based on sodium alginate (SA) modified by a FeBTC metal–organic framework were developed for isopropanol dehydration using a membrane process, pervaporation. Two kinds of SA-FeBTC membranes were developed: (1) untreated membranes and (2) cross-linked membranes with citric acid or phosphoric acid. The structural and physicochemical properties of the developed SA-FeBTC membranes were studied by spectroscopic techniques (FTIR and NMR), microscopic methods (SEM and AFM), thermogravimetric analysis and swelling experiments. The transport properties of developed SA-FeBTC membranes were studied in the pervaporation of water–isopropanol mixtures. Based on membrane transport properties, 15 wt % FeBTC was demonstrated to be the optimal content of the modifier in the SA matrix for the membrane performance. A membrane based on SA modified by 15 wt % FeBTC and cross-linked with citric acid possessed optimal transport properties for the pervaporation of the water–isopropanol mixture (12–100 wt % water): 174–1584 g/(m^2 h) permeation flux and 99.99 wt % water content in the permeate.

Keywords: mixed matrix membrane; sodium alginate; FeBTC; pervaporation; isopropanol

Citation: Kuzminova, A.; Dmitrenko, M.; Mazur, A.; Ermakov, S.; Penkova, A. Novel Pervaporation Membranes Based on Biopolymer Sodium Alginate Modified by FeBTC for Isopropanol Dehydration. *Sustainability* **2021**, *13*, 6092. https://doi.org/10.3390/su13116092

Academic Editors: Elena Cristina Rada and Vincenzo Torretta

Received: 7 April 2021
Accepted: 26 May 2021
Published: 28 May 2021

1. Introduction

Currently, modern society strives for the development of sustainable processes that are aimed at meeting human needs while preserving the environment. In recent years, the requirements for the characteristics of substances, such as quality, purity and environmental friendliness, have been increasing. Therefore, the development of energy-efficient methods and materials, as well as purification technologies, is becoming more popular [1–3]. Membrane technologies meet all of the requirements for "sustainable processes" and are of great interest due to the following advantages: cost-effectiveness, environmental friendliness, the absence of additional reagents and the ease of use over traditional separation methods [4–7]. Pervaporation is a common membrane method for the separation of low-molecular-weight components in thermally unstable mixtures, as well as azeotropic mixtures and mixtures of isomers. Pervaporation is often used for the dehydration of alcohols. Alcohols are widely used in various fields of industry, in particular chemicals, food, pharmaceuticals, etc. Isopropanol/water is a widespread model to study water–alcohol mixtures. Since this mixture contains an azeotrope with a water content of 12 wt % and a boiling point of 80.3 °C [8], it is difficult to separate by traditional methods. Moreover, traditional separation techniques, as a rule, do not correspond to "sustainable processes". The rapid development of this method requires the search for new membrane materials with the desired properties. There are two large classes of membrane materials usually

used for pervaporation dehydration, ceramic and polymeric. Ceramic membranes have high chemical and thermal resistance and a lack of plasticization. However, they also has some disadvantages, such as fragility, high cost and poor reproducibility of transport characteristics [9]. The second type is polymeric membranes, which have good film formation, mechanical properties, price and reproducibility of transport characteristics, but low permeability or selectivity. For the pervaporation of isopropanol–water mixtures, ceramic [10,11], hydrophilic pervaporation polymeric membranes [12–23] and commercial membranes based on PVA (Pervap 2201, Sulzer Chemtech, Allschwil, Switzerland), amorphous perfluorinated polymers (CMS, Compact Membrane Systems) and those based on aromatic polyamide (reverse osmosis membranes—SWC5, ESPA2 and CPA5, Japan) [24–26] were applied. The following polymeric membrane materials are widely employed: polyvinyl alcohol (PVA) [12,13], sodium alginate (SA) [14–18], polyvinyl amine [19], chitosan [20–22], poly(ionic liquid) complex (PILC) [23], etc. However, it is worth noting that polymer membranes suffer from a permeation flux/selectivity trade-off, i.e., a high separation factor is combined with a relatively low permeation flux or vice versa [27,28]. This problem and the rapid development of technologies focused on environmental protection, the economy and the industrial sector, has led to the development of novel pervaporation membranes based on high-performance composite materials. A composite, as a rule, consists of at least two materials, one of which is a matrix and the other of which is a filler (modifier); such a combination provides the advantages of both components of the composite [29]. Thus, composite materials are often used to create mixed matrix membranes for the pervaporation with the aim of obtaining tailored transport characteristics and preventing the permeability/selectivity trade-off.

In this work, a widely used water-soluble biopolymer, sodium alginate (SA), was chosen as the polymer matrix, since the membrane materials on the basis of SA meet all the requirements of a "sustainable process". SA is extracted from brown algae that grow in cold-water regions [30] and is widely used as a membrane material for the production of membranes due to its unique chemical and mechanical properties, good film formation, low cost, etc. The following applications of SA as a membrane material have been described in the literature: ultrafiltration [31], pervaporation [14,18,32–38] and nanofiltration [39,40], as well as a polyelectrolyte [41–43]. Different fillers such as dextrin [44], metal oxides [45–48], glycogen [49], graphene oxide [50], covalent organic frameworks [51,52], fullerenol [14], zeolites [34,53] and metal–organic frameworks (MOFs) [18,36,54–57] are used to improve SA membrane characteristics. MOFs are promising fillers for creating mixed matrix membranes due to their unique design and simplicity of modification, and the high compatibility between the polymer matrix and the filler [58]. The use of MOFs as a modifier affects the hydrophilic/hydrophobic balance of the surface, the free volume and the sorption characteristics of the polymer matrix due to the porous structure of the MOFs [18]. MOFs are used as modifiers for polymer membranes in such membrane processes as ultrafiltration [59–63], nanofiltration [64–70], pervaporation [13,18,36,54–57,71–94], etc.

MOFs were shown to be capable of improving the transport properties of pervaporation membranes based on chitosan [83,84,92], polydimethylsiloxane (PDMS) [77,78], polyimide [79,80], polyamide [91], polyarylethersulfone [82], PVA [13,85–88], poly(ethyleneimine) [94], polyether-block-amide (PEBA) [81], cardo polyetherketone (PEK-c) [93], etc. For the modification of pervaporation membranes based on SA, the following MOFs were tested in previous publications: $[Eu(BTB)(H_2O)_2 \cdot solvent]_n$ [55], FeIII-HMOF-5 [57], hollow zeolitic imidazolate framework-8 (HZIF-8) [36], zeolitic imidazolate frameworks ZIF-L and ZIF-8 [56], NH_2-MIL-125(Ti) [54], Zr-MOFs (UiO-66, UiO-66(NH_2)-AcOH and UiO-66(NH_2)-EDTA) [18]. The improvement of pervaporation SA membranes is associated with the porous and hydrophilic/hydrophobic structure of MOF nanoparticles, and increased sorption of water due to the presence of metal ions.

To the best of our knowledge, there is no information about pervaporation membranes based on SA modified with FeBTC particles. FeBTC is an unconventional representative of the MOF class due to its semi-crystalline/semi-amorphous nature [95]; moreover, this

MOF is commercially available and is produced under the brand Basolite F300. FeBTC is an iron (III) trimesate (Fe (III) and 1,3,5-benzoletricarboxylate) with a microporous structure (window sizes 5.5 and 8.6 A) [96]. FeBTC has high chemical stability, in particular, in air [97], water [97] and organic solvents [98], which makes this structure suitable for use as a filler for polymer membranes. FeBTC was successfully applied as a filler for a pervaporation membrane based on polylactic acid for the separation of a methanol/methyl tert-butyl ether (MTBE) mixture [99]. To the best of our knowledge, there are no data in the literature on the use of FeBTC for the modification of water-soluble pervaporation polymer membranes for dehydration.

The aim of the present work was to develop novel green membranes based on SA modified by FeBTC for the pervaporation dehydration of isopropanol. We were able to improve the transport properties of the developed dense SA-FeBTC membranes through modification, due to the following properties of the used MOF: porous structure of FeBTC, stability in water and organic solvent and hydrophobic/hydrophilic properties. All that affects the sorption characteristics, free volume and surface of the developed membranes. Two kinds of SA-FeBTC membranes were developed: (1) untreated membranes and (2) cross-linked membranes with citric acid or phosphoric acid. The structural and physicochemical properties of the developed untreated and cross-linked SA-FeBTC membranes were studied by spectroscopic techniques (FTIR and NMR), microscopic methods (SEM and AFM), thermogravimetric analysis (TGA) and swelling experiments. The transport properties of the developed SA-FeBTC membranes were studied in the pervaporation of water–isopropanol (30/70 wt %) mixtures for untreated membranes, and in the pervaporation of water–isopropanol with 12–100 wt % water for cross-linked membranes.

2. Materials and Methods

2.1. Materials

Sodium alginate SA (viscosity of 90 cps, BIOPROD, St. Petersburg, Russia) was used as the membrane material. FeBTC (Basolite F300, produced by BASF), purchased from Sigma–Aldrich (St. Petersburg, Russia), was used as a modifier for the SA modification. Isopropanol (i-PrOH) and citric and phosphoric acids (Vekton, St. Petersburg, Russia), used to cross-link the SA-based membranes, were applied without further purification.

2.2. Dense Membrane Preparation

To prepare unmodified membranes, an SA solution was prepared at 45 °C for 5 h with constant stirring using a magnetic stirrer. The SA-FeBTC composites were prepared by the solid-phase method by simultaneous grinding and mixing of SA and FeBTC in an agate mortar. Up to 20 wt % FeBTC with respect to the polymer weight, was added to the polymer matrix. The resulting SA-FeBTC mixture was dissolved in distilled water at 45 °C for 5 h with constant stirring using a magnetic stirrer. Next, the SA and SA-FeBTC solutions obtained were sonicated at room temperature and poured into Petri dishes for subsequent preparation of dense membranes. Dense membranes were prepared by solvent evaporation in an oven at 40 °C for 24 h. The thickness of the dense SA and SA-FeBTC membranes, measured with a micrometer, was 25 ± 3 μm.

To use the membranes over the entire concentration range, the polymer chains of the developed SA and SA-FeBTC membranes were cross-linked with citric or phosphoric acids. For this purpose, the polymer films were immersed in a solution of 3.5 wt % citric or 3.5 vol % phosphoric acid in water/isopropanol (30/70 wt % or 10/90 vol %, respectively) mixture for 180 min at room temperature. The remaining acids were removed with deionized water. After that, the dense membranes were ready for further use. Table 1 shows the designations of membranes developed in this work.

Table 1. Developed dense membranes based on SA and SA-FeBTC composites.

Membrane	Thickness, μm	Content of FeBTC, wt.%	Cross-Linking Method
SA-0	25	0	–
SA-5	25	5	–
SA-10	25	10	–
SA-15	25	15	–
SA-20	25	20	–
SA-0/CA	25	0	3.5 wt % citric acid
SA-15/CA	25	15	3.5 wt % citric acid
SA-0/PA	25	0	3.5 vol % phosphoric acid
SA-15/PA	25	15	3.5 vol % phosphoric acid

2.3. Fourier Transform Infrared Spectroscopy (FTIR)

Structural changes in the SA and SA-FeBTC membranes were studied using a BRUKER-TENSOR 27 spectrometer (Shimadzu, St. Petersburg, Russia), to which an attenuated total reflectance (ATR) accessory was attached. The measurement was carried out at 25 °C in the range of 600–4000 cm^{-1}.

2.4. Nuclear Magnetic Resonance (NMR)

NMR was carried out using a Bruker Avance III 400 WB NMR spectrometer (Bruker, Ettlingen, Germany) with a 3.2 mm CP/MAS probe, magnetic field 9.4 T and Larmor frequency of 100.64 MHz. The NMR experiments were carried out in a 3.2-mm zirconium oxide rotor, which was spun at 12.5 kHz. $\{1H\}^{13}C$ CP/MAS NMR spectra were collected for 8192 sample scans, with a contact time of 2 ms and a relaxation time of 5 s. Liquid tetramethylsilane (TMS) was used as an external reference for ^{13}C nuclei.

2.5. Scanning Electron Microscopy (SEM)

The inner morphology and surface of dense SA and SA-FeBTC membranes were studied by SEM on a Zeiss AURIGA Laser at 1 kV (Carl Zeiss SMT, Oberhochen, Germany). Cross-sections of the membranes were obtained by breaking the membrane perpendicular to the surface in liquid nitrogen.

2.6. Atomic Force Microscopy (AFM)

Atomic force microscope NT-MDT NTegra Maximus (standard silicon cantilevers, rigidity of 15 $N \cdot m^{-1}$ in tapping mode) was used to investigate the surface topography of the SA and SA-FeBTC membranes (NT-MDT Spectrum Instruments, Moscow, Russia).

2.7. Swelling Measurements

The equilibrium swelling degree (sorption) was studied in an isopropanol/water azeotropic mixture, in a 30/70 wt % water/isopropanol mixture for the untreated and cross-linked SA and SA-FeBTC membranes, as well as in water for cross-linked SA and SA-FeBTC membranes by the gravimetric method at 25 °C. Each membrane was put into a weighing bottle and the weight of the membranes was checked regularly until complete swelling.

To calculate the swelling degree, *S*, Equation (1) was used:

$$S = \frac{m_s - m_o}{m_o} * 100\% \quad (1)$$

where m_s (g) is the weight of the swollen membrane and m_o (g) is the initial weight of the dry membrane.

2.8. Thermogravimetric Analysis (TGA)

The thermochemical properties of the SA and SA-FeBTC membranes were studied by thermogravimetric analysis (TGA) on a Thermobalance TG 209 F1 Libra (Netzsch, Leuna,

Germany) in the heating temperature range from 37 to 570 °C at a heating rate of 10 °C/min in an argon atmosphere.

2.9. Pervaporation Experiment

The transport properties of the developed dense SA and SA-FeBTC membranes were studied in a laboratory cell for pervaporation with an effective membrane area of 9.6×10^{-4} m^2 in a stationary mode with residual pressure under a membrane of 0.2 mbar with stirring at 22 °C [18]. In pervaporation experiments, the first permeate sample was collected after 30 min and not analyzed, since during this time the initial swelling of the membrane in the feed and the membrane preconditioning were achieved [100,101]. The following permeate samples were collected during various time periods (from 10 min to 3 h) depending on the performance of the membrane, but the permeate weight was above 0.3 g to obtain reliable data on membrane selectivity and permeate composition. The composition of the permeate and the feed was investigated on a Chromatec Crystal 5000.2 gas chromatograph (Chromatec, Nizhny Novgorod, Russia) on a "Hayesep R" column with a thermal conductivity detector; the column was 2 m long and 3 mm in diameter.

The permeation flux J (kg/(m^2h)) of the dense SA and SA-FeBTC membranes was calculated as described previously [102]:

$$J = \frac{W}{A \cdot t} \tag{2}$$

where W (kg) is the mixture weight that permeated through the membrane, A (m^2) is the effective membrane area and t (h) is the time of the measurement.

The normalized permeation flux J_n (kg/(m^2·h·μm)) of the dense SA and SA-FeBTC membranes was calculated by the following equation:

$$J_n = J/l \tag{3}$$

where J is the permeation flux and l is membrane thickness.

Additionally, such parameters as the separation factor (β), component permeances (P/l) and pervaporation separation index (PSI) were calculated to assess the effectiveness of membranes.

The separation factor (β) was calculated by the following equation [103]:

$$\beta = \frac{y_i/y_j}{x_i/x_j} \tag{4}$$

where y_i and y_j are the weight of the components i and j in the permeate; x_i and x_j are the weight of the components i and j in the feed.

The permeance P/l was determined as previously described by Baker et al. [103]:

$$P/l = \frac{j_i}{p_{i_f} - p_{i_p}}, \tag{5}$$

where j_i is the partial flux of component i; l is the membrane thickness; and p_{i_f} and p_{i_p} are the vapor pressures of component i in the feed and the permeate, respectively. Gas permeation units (GPU) were used to express the permeances of the water and isopropanol (1 GPU = 1×10^{-6} cm^3 (STP)/cm^2 s cm Hg; 1 m^3 m/m^2 s kPa = 1.33×10^8 GPU).

The pervaporation separation index (PSI) was calculated by the following equation:

$$\text{PSI} = J \cdot (\beta - 1). \tag{6}$$

To ensure the accuracy of all assessed parameters, data were collected in triplicate and for subsequent presentation the average value was used. A series of one type of membrane was always prepared. Each membrane from this series was tested separately in a pervaporation unit under certain conditions. Every untreated (uncross-linked) membrane from one series was studied by pervaporation at one concentration of the water–isopropanol (30/70 wt %) mixture, collecting several permeate and retentate samples. Every cross-linked membrane from one series was studied by continuous pervaporation at the series of water concentration in the feed (12–100 wt % water): several permeate and retentate

samples at a certain feed concentration were collected, and the concentration of water in the mixture was increased and studied in the same way. The obtained average accuracies were ±0.5% for water content in the permeate and ±5% for the permeation flux for the dense SA and SA-FeBTC membranes.

3. Results

Based on the conducted pervaporation experiments on isopropanol dehydration (Section 3.2.1), the optimal content of the modifier FeBTC in SA matrix was chosen 15 wt % due to the improved transport characteristics. Thus, the study of the structure and physicochemical properties (Section 3.1) is presented, in particular, for membranes modified with 15 wt % FeBTC.

3.1. Structure and Physicochemical Properties Investigation of Untreated and Cross-Linked SA and SA-FeBTC Membranes

3.1.1. Fourier Transform Infrared Spectroscopy (FTIR)

FTIR spectroscopy was used to study the structural changes of the untreated and cross-linked membranes based on SA and the composite containing 15 wt % FeBTC in the SA matrix. The IR spectra of the untreated and cross-linked SA-0 and SA-15 membranes are shown in Figure 1.

The IR spectrum for the SA-0 membrane (Figure 1a) shows a broad band at 3251 cm^{-1} and a minor peak with a maximum at 2918 cm^{-1}, which correspond to vibrations of O–H and C–H bonds, respectively. In the low-frequency region, two pronounced peaks are observed at 1591 cm^{-1} and 1406 cm^{-1}, which correspond to symmetric and asymmetric stretching vibrations of the carboxylate group, respectively. The high-intensity peak at 1022 cm^{-1} corresponds to overlapping stretching vibrations from alcohol and ether groups for C–O. The broad band at 674 cm^{-1} may be associated with O–H out-of-plane vibrations. After the introduction of FeBTC into the SA matrix, the peak at 3251 cm^{-1} corresponding to the O–H groups decreases. The bands with maxima at 1631 and 1450 cm^{-1} correspond to the –C=O asymmetric and symmetric stretching vibrations of organic ligands, respectively [104]. These changes may indicate the formation of hydrogen and electrostatic bonds between the polymer and the FeBTC modifier [57].

For the SA-0/CA membrane (Figure 1b), a broadening of a peak at 1597 cm^{-1} and the presence of a peak at 1238 cm^{-1} are observed, which correspond to the stretching of C=O and C–O–C ether bonds between the rings in the main chain of SA, respectively. These changes compared to the SA-0 membrane (Figure 1a) indicate the cross-linking of the SA chains with citric acid [105]. A small peak in the range of 1300–1400 cm^{-1} for the SA-0/PA membrane (Figure 1c) corresponds to the specific absorption of the –C–O–P– bond, which confirms the cross-linking of the SA chains with phosphoric acid [105]. Furthermore, for the cross-linked SA-0/CA and SA-0/PA membranes, peaks are observed at 1725 and 1720 cm^{-1}, respectively, confirming the formation of ester bonds during the cross-linking reaction between CA, PA hydroxyl and SA carboxyl groups [105]. After the introduction of 15 wt % FeBTC into the SA matrix and cross-linking of the membranes with acids (Figure 1b,c), the spectra also show characteristic peaks of the MOF.

3.1.2. Nuclear Magnetic Resonance (NMR)

NMR spectra of the untreated and cross-linked membranes based on SA and SA-FeBTC (15%) composite, decomposed into components, are shown in Figures 2 and 3, respectively.

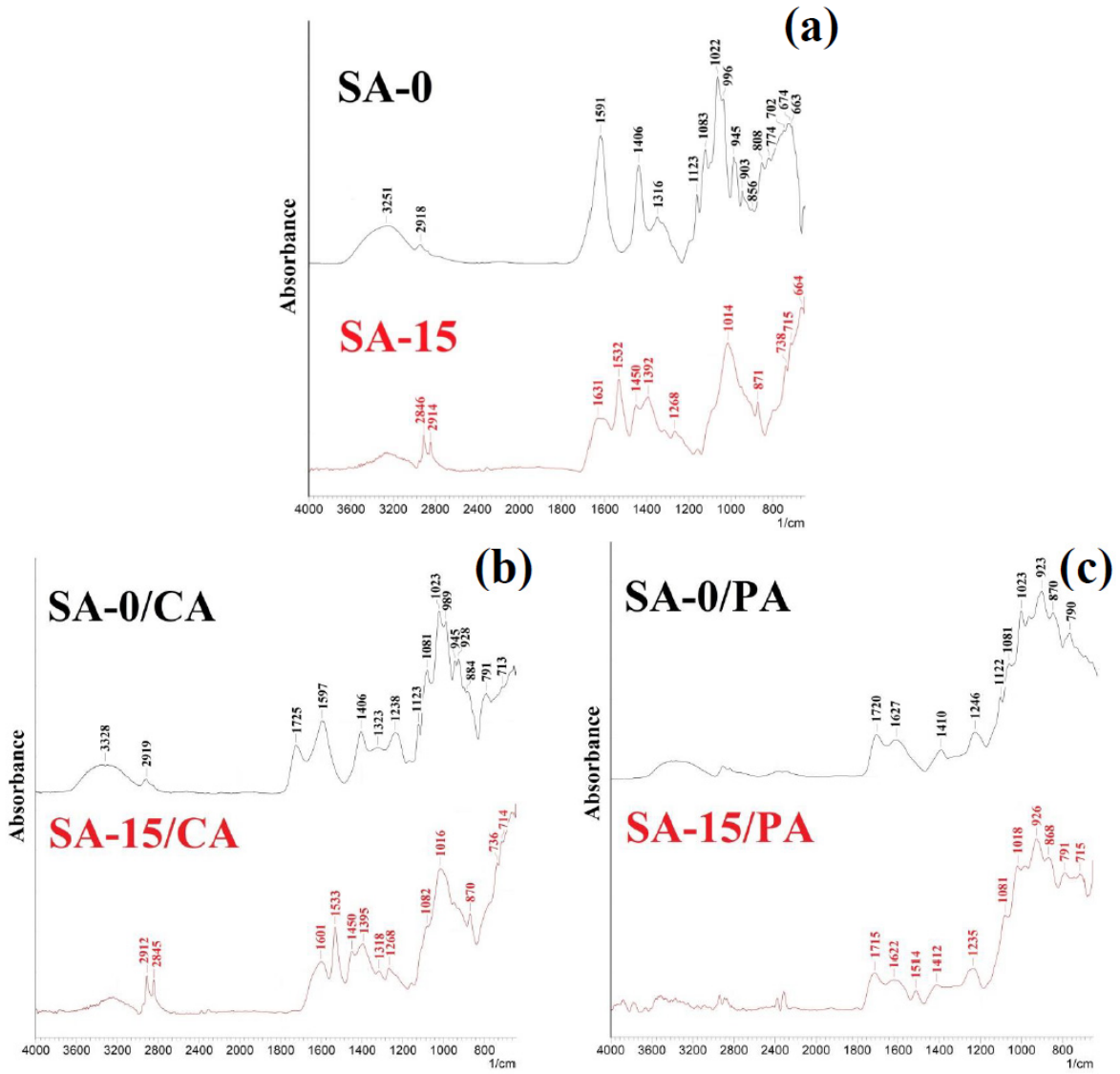

Figure 1. IR spectra of untreated cross-linked membranes: (**a**) SA-0 and SA-15, (**b**) SA-0/CA and SA-15/CA, (**c**) SA-0/PA and SA-15/PA.

The spectrum of the SA-0 membrane presented in Figure 2a demonstrates that the degree of membrane crystallinity is 49% (based on the ratio of integral areas of the spectrum components in the region of 90–110 ppm). For the membranes cross-linked with acids (Figure 2b,c), the spectral lines of carboxyl carbon atoms exhibit inhomogeneous broadening in the form of an additional component at about 174 ppm. This behavior can be associated with the substitution of sodium ions by hydrogen during the reduction process (the protonation of the carboxyl group). Thus, it can be concluded that SA remains intact about 12% for the SA-0/CA (Figure 2b) and 14% for the SA-0/PA (Figure 2c) according to the line area in the range 160–190 ppm. Furthermore, cross-linking of the membranes decreases the degree of crystallinity to 39% for the SA-0/CA and 29% for the SA-0/PA. For the SA-0/PA membrane (Figure 2c), a low-intensity spectral component of about 71 ppm appears of the spectrum, which may correspond to the formation of a bond with phosphoric acid –C–O–P–, which was also confirmed by the FTIR data (Figure 1). Moreover, the relative abundance of such functional groups is about 2–3%.

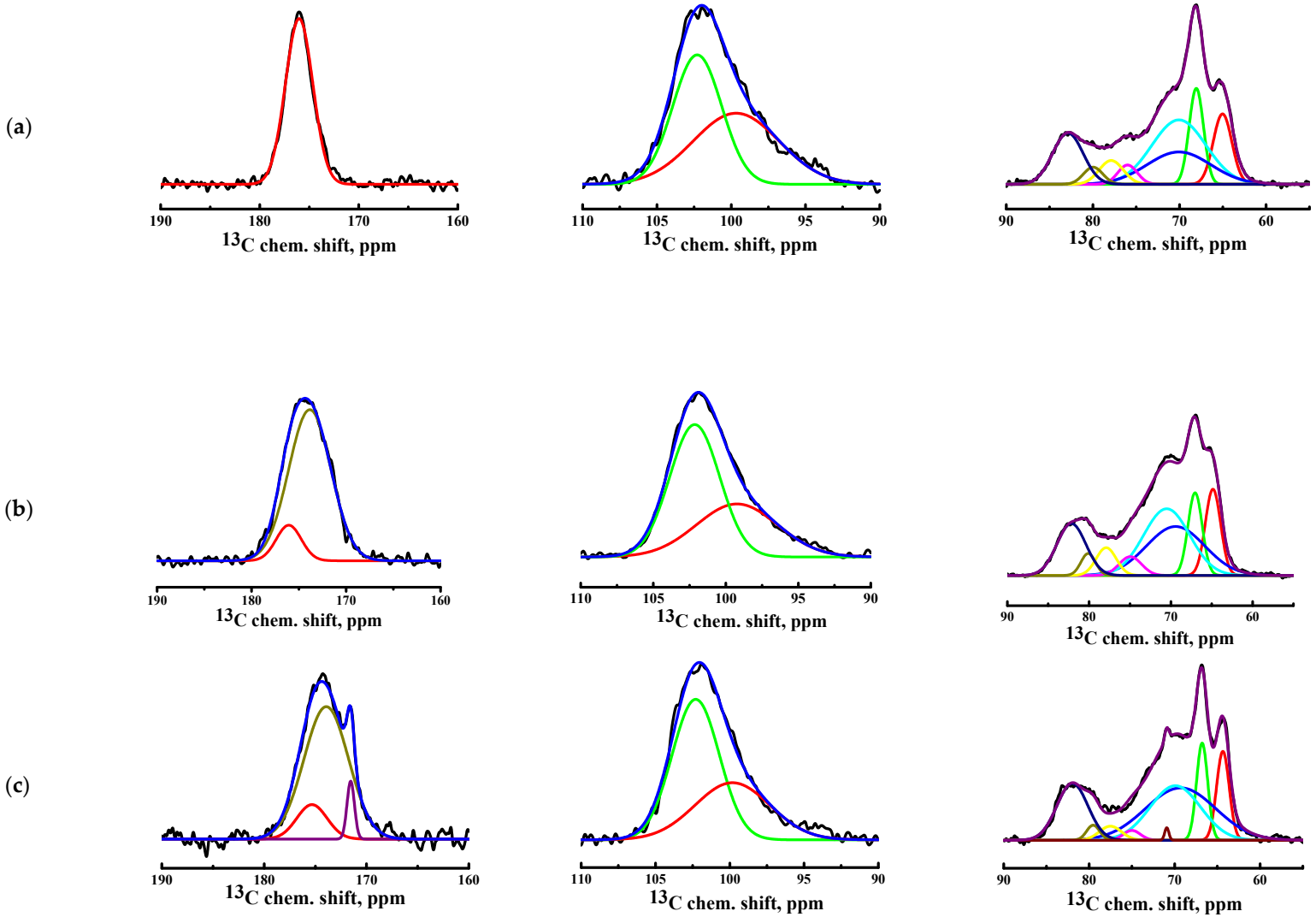

Figure 2. ^{13}C NMR spectra of the untreated and cross-linked SA membranes, decomposed into components: (**a**) SA-0, (**b**) SA-0/CA and (**c**) SA-0/PA.

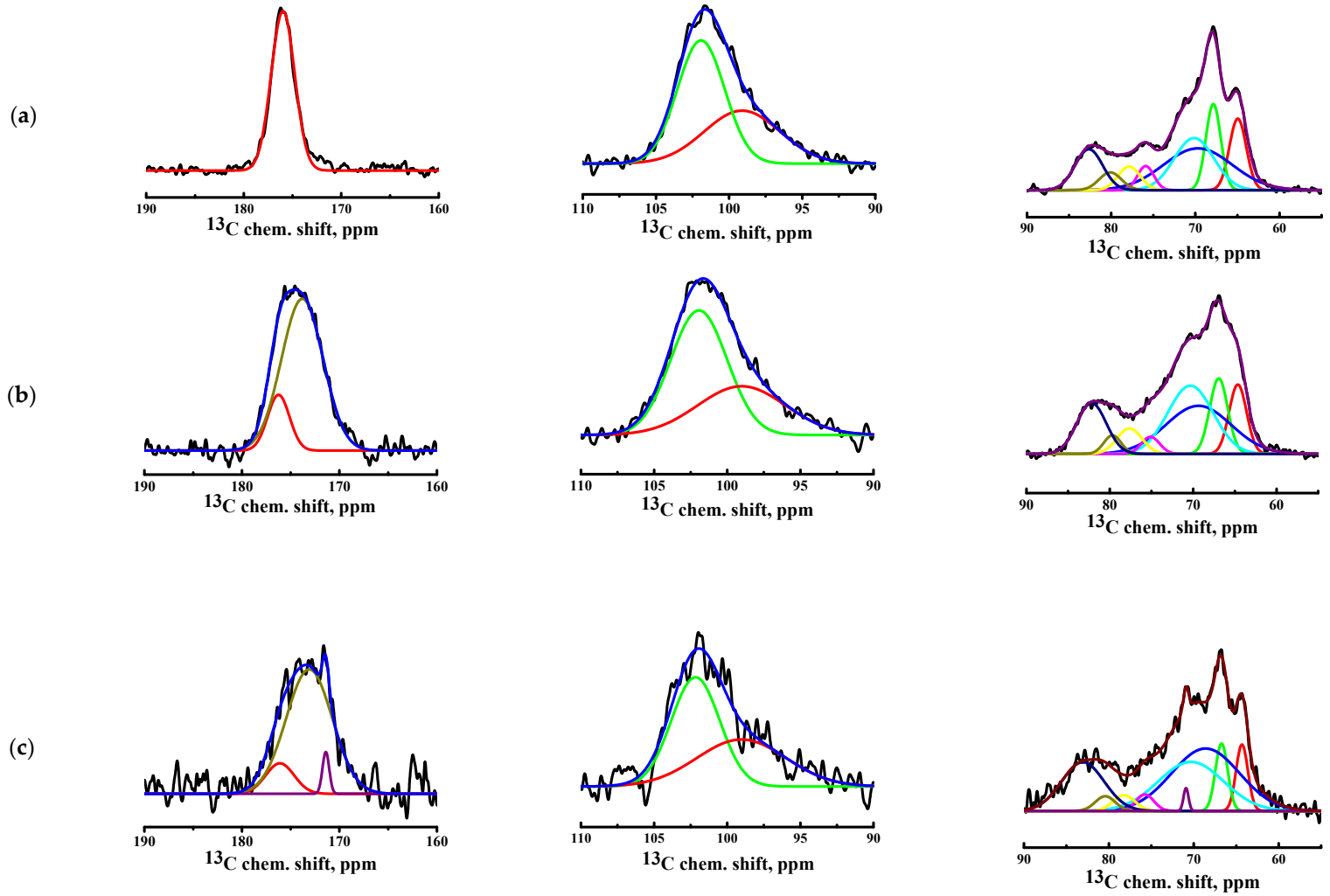

Figure 3. ^{13}C NMR spectra of the untreated and cross-linked SA-FeBTC (15%) membranes, decomposed into components: (**a**) SA-15, (**b**) SA-15/CA and (**c**) SA-15/PA.

Figure 3 shows ^{13}C NMR spectra of the untreated and cross-linked membranes based on the SA-FeBTC (15 wt %) composite. Spectral components in the range of 90–110 ppm (Figure 3a) indicate that the introduction of FeBTC does not affect the chemical nature of SA but reduces the degree of crystallinity to 30% due to the FeBTC semi-amorphous structure, resulting in the increased permeability of the modified SA-15 membrane (Figure 9). The addition of FeBTC has a small effect on the reduction of carboxyl groups when exposed to acids. In particular, the amount of residual sodium ions is 17% for SA-15/CA (Figure 3b) and 13% for SA-15/PA (Figure 3c). The degree of crystallinity of the SA-15/CA membrane hardly changed, remaining at 38% compared to the SA-0/CA membrane, while for SA-15/PA it increased to 44% compared to the SA-0/PA membrane (Figure 2b,c). At the same time, the number of –C–O–P– groups remained practically unchanged and amounted to 3%.

3.1.3. Thermogravimetric Analysis (TGA)

The thermal stability of the untreated and cross-linked membranes based on SA and the SA-FeBTC composite was investigated by TGA. The obtained thermograms are presented in Figure 4.

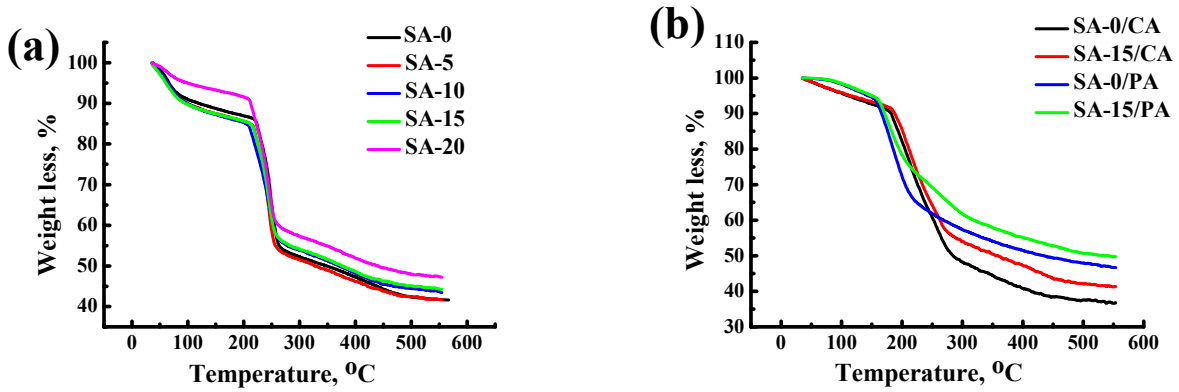

Figure 4. Thermogravimetric curves for the SA and SA-FeBTC membranes: (**a**) untreated and (**b**) cross-linked.

Figure 4a shows three stages of weight loss for all untreated membranes in the following temperature ranges: (1) 35–210 °C; (2) 210–260 °C; and (3) >260 °C. The first stage of weight loss is attributed to the evaporation of desorbed water in membranes [16]; the weight loss for all untreated membranes was approximately the same and equaled 10–15% at 210 °C. The second stage corresponds to the thermal decomposition of carboxyl and hydroxyl groups, while the final weight loss step corresponds to the decomposition of the polymer backbones [51]. The introduction of FeBTC increased the thermal stability of SA membranes proportionally to the content of MOF in the polymer matrix. So, the weight loss for the SA-0 membrane was 58.3%, while for the SA-20 membrane it was 52.7% at 550 °C.

For the cross-linked membranes (Figure 4b), three areas of weight loss are also observed: for membranes cross-linked with citric acid: (1) 35–180 °C, (2) 180–290 °C, (3) >290 °C; for membranes cross-linked with phosphoric acid: (1) 35–160 °C, (2) 160–210 °C, (3) >210 °C. At the same time, weight loss for the cross-linked membranes is smoother than that for the untreated ones. The use of phosphoric acid for cross-linking increased thermal stability (weight loss at 550 °C for the SA-0/PA and SA-15/PA membranes was 53.3% and 50.3%, respectively), compared to citric acid (weight loss at 550 °C for the SA-0/CA and SA-15/CA membranes was 63.4% and 58.8%, respectively). This was related to the stronger cross-linking of the polymer chains by PA (confirmed by swelling data in water in Section 3.1.6). It is also worth noting that the cross-linked membranes modified with FeBTC (SA-15/PA and SA-15/CA) had a higher thermal stability (reduced weight loss) than the unmodified cross-linked membranes (SA-0/PA and SA-0/CA).

3.1.4. Scanning Electron Microscopy (SEM)

The inner structure of the untreated and cross-linked SA and SA-FeBTC membranes was studied by SEM. The cross-sectional and surface SEM micrographs for untreated and cross-linked SA and SA-FeBTC membranes are presented in Figures 5 and 6, respectively.

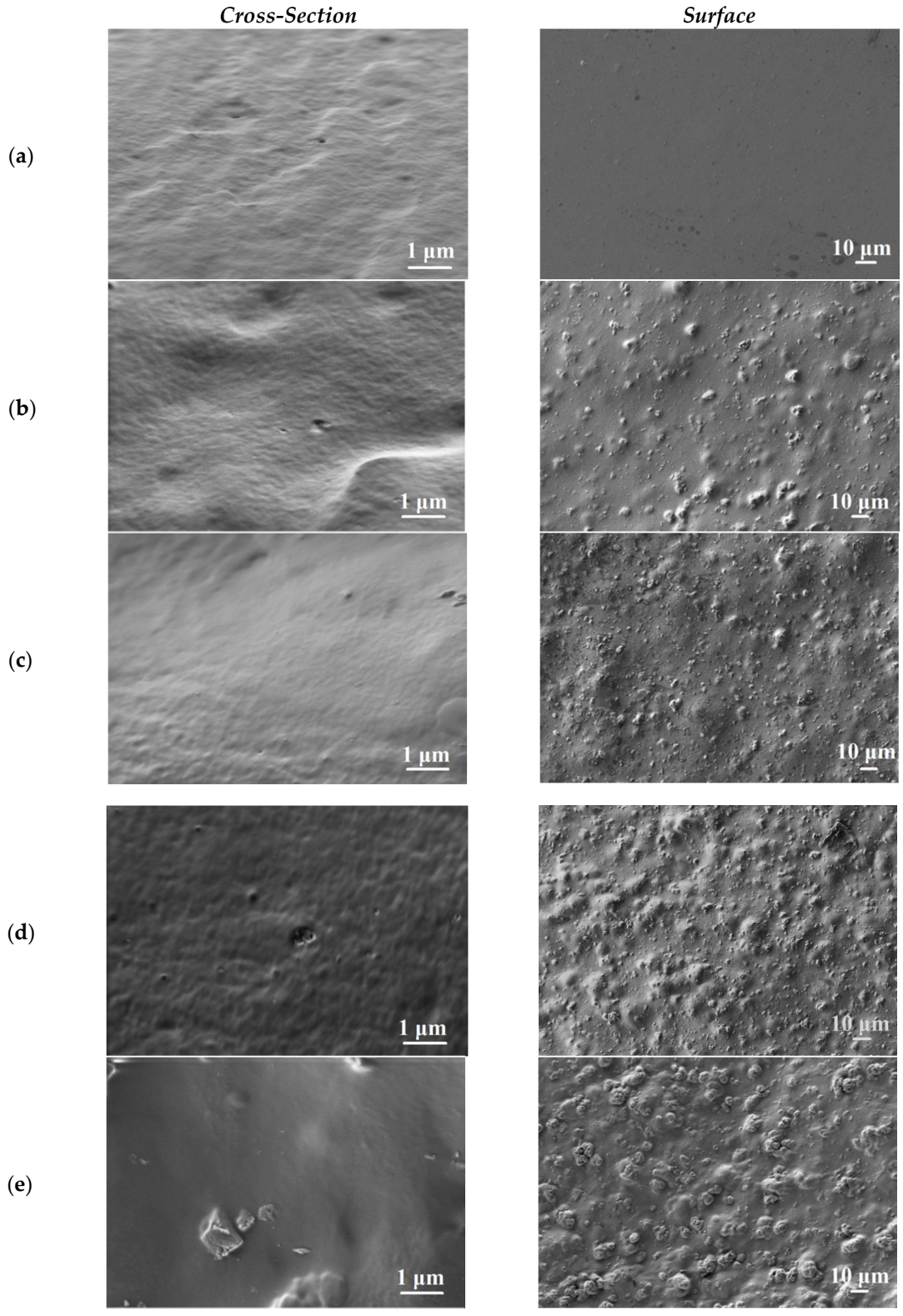

Figure 5. The cross-sectional and surface SEM micrographs of the untreated SA and SA-FeBTC membranes: (**a**) SA-0, (**b**) SA-5, (**c**) SA-10, (**d**) SA-15 and (**e**) SA-20.

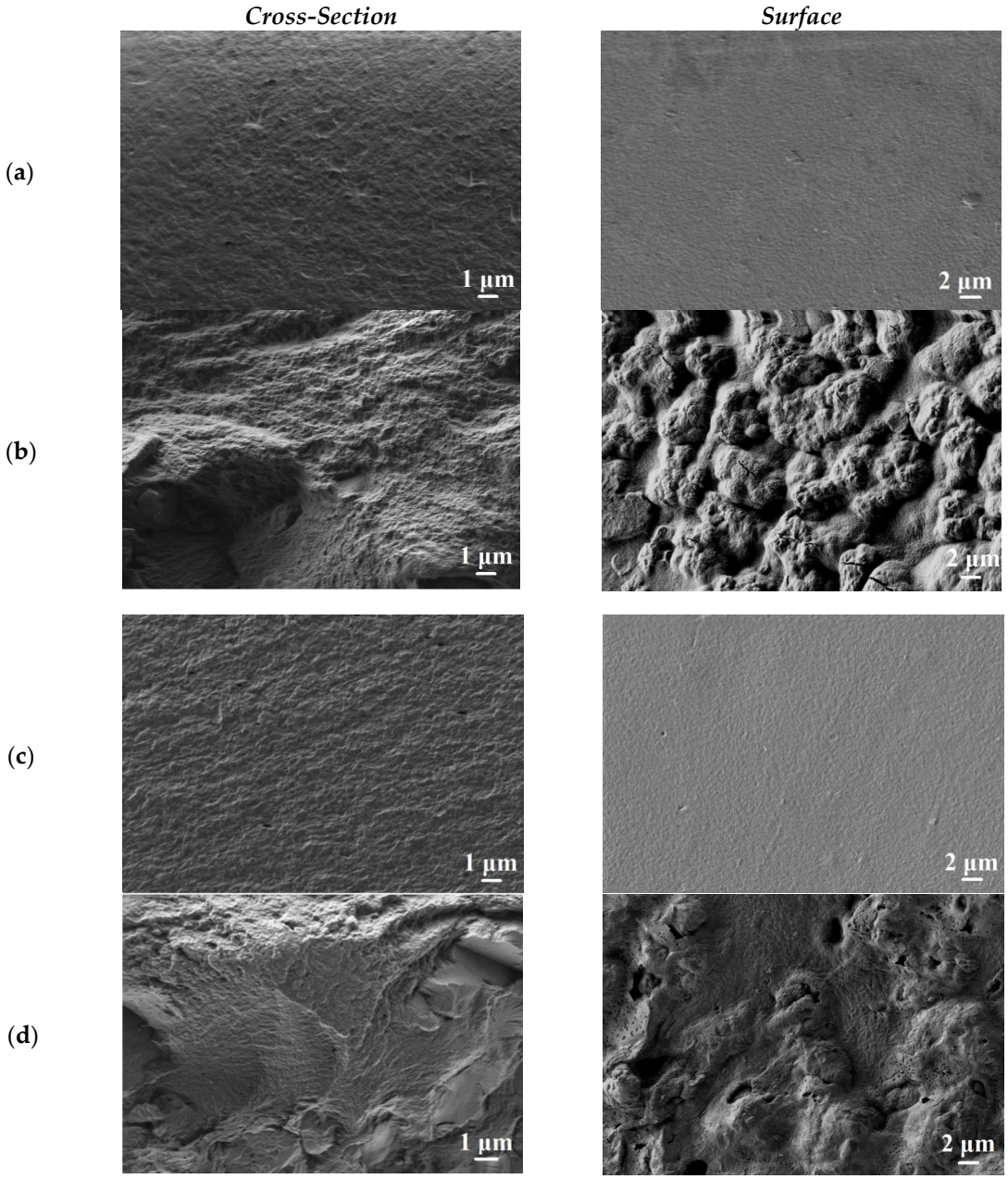

Figure 6. The cross-sectional and surface SEM micrographs of the cross-linked SA and SA-FeBTC membranes: (**a**) SA-0/CA, (**b**) SA-15/CA, (**c**) SA-0/PA and (**d**) SA-15/PA.

The presented SEM micrographs show the smooth structure of the cross-section and surface for the SA-0 membrane (Figure 5a). The introduction of up to 15 wt % FeBTC does not significantly change the cross-sectional structure, while at 20 wt % FeBTC (for SA-20 membrane), the particles are clearly visible on the cross-section. The introduction of FeBTC modifies the membrane surface: with an increase in the FeBTC content, the number of agglomerates increases on the membrane surface.

The cross-linking of the membranes based on pure SA with acids results in a "rougher" cross-section with small plastic deformations (Figure 6a,c) compared to the untreated SA-0 membrane (Figure 5a). The membrane surface (Figure 6a,c) remains practically unchanged when polymer chains are cross-linked with acids compared to the untreated SA-0 membrane (Figure 5a). The introduction of 15 wt % FeBTC and cross-linking with acids significantly changed the cross-sectional structure, with a large number of great plastic deformations and irregularities compared to the unmodified cross-linked membranes.

It should be noted that the cross-section is coarser (with larger modifications) for the membrane cross-linked with phosphoric acid (SA-15/PA, Figure 6d) than for the membrane cross-linked with CA (SA-15/CA, Figure 6b). For the SA-15/PA and SA-15/CA membranes, FeBTC particles are visible on the membrane surface, resulting in a rough surface structure compared to the unmodified cross-linked membranes. Moreover, for the SA-15/CA membrane, more particles and a rougher surface are observed, which generates more sorption centers for the feed components on the membrane surface, leading to the highest values of permeation flux (Figure 10a).

3.1.5. Atomic Force Microscopy (AFM)

The surface roughness of the untreated and cross-linked SA and SA-FeBTC membranes was studied by AFM. AFM images with a scan size of 100 µm × 100 µm for the membranes under study are presented in Figures 7 and 8, respectively.

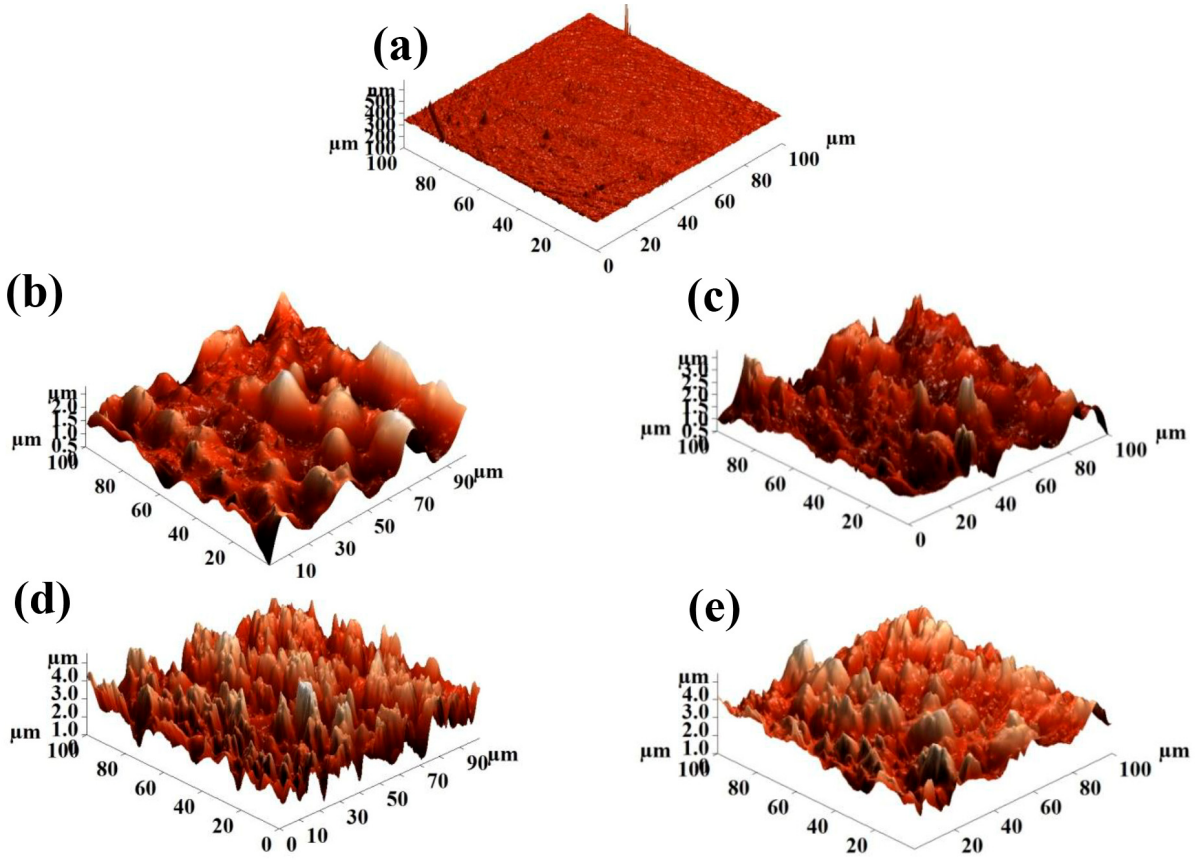

Figure 7. AFM images of the untreated SA and SA-FeBTC membranes: (**a**) SA-0, (**b**) SA-5, (**c**) SA-10, (**d**) SA-15 and (**e**) SA-20.

The surface roughness characteristics (average roughness (Ra) and root mean square roughness (Rq)) of the untreated SA and SA-FeBTC membranes were calculated based on the AFM images (Figure 7) and are presented in Table 2.

Table 2. The values of average roughness (Ra) and root mean square roughness (Rq) of the untreated SA and SA-FeBTC membranes.

Membrane	Ra, nm	Rq, nm
SA-0	4.8	7.9
SA-5	279.9	358.9
SA-10	327.2	418.3
SA-15	416.4	520.9
SA-20	424.4	536.5

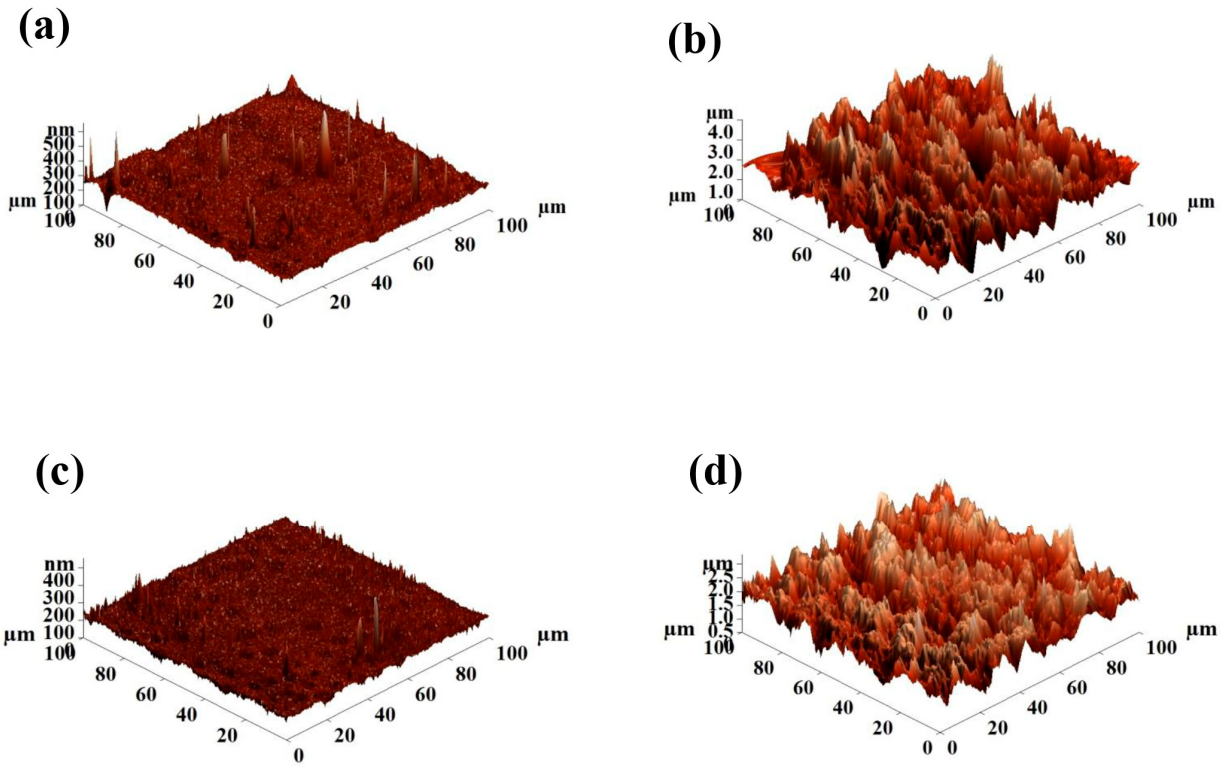

Figure 8. AFM images of the cross-linked SA and SA-FeBTC membranes: (**a**) SA-0/CA, (**b**) SA-15/CA, (**c**) SA-0/PA and (**d**) SA-15/PA.

The data presented in Table 2 demonstrate that the introduction of FeBTC into the SA matrix significantly increases the values of average roughness (Ra) and root mean square roughness (Rq), with a rise in the modifier content in the polymer matrix. The maximum values of Ra and Rq are observed for the SA-20 membrane (88.4-fold increase in Ra and 67.9-fold increase in Rq compared to the untreated SA-0 membrane), due to the highest agglomeration of FeBTC particles being on the membrane surface (confirmed by SEM data, Figure 5e). The roughness of the membrane surface affects the sorption of the components of the mixture to be separated. For the SA-15 and SA-20 membranes, close values of surface roughness parameters were observed. However, the SA-20 membrane had a lower permeability compared to the SA-15 membrane (Figure 9), which was related to the large degree of nanoparticle agglomeration on the surface causing hindered transport of the feed components through the membrane.

The surface roughness characteristics (average roughness (Ra) and root mean square roughness (Rq)) of the cross-linked SA and SA-FeBTC membranes were calculated based on the AFM images (Figure 8) and are presented in Table 3.

Table 3. The values of average roughness (Ra) and root mean square roughness (Rq) of the cross-linked SA and SA-FeBTC membranes.

Membrane	Ra, nm	Rq, nm
SA-0/CA	11.3	20.6
SA-15/CA	477.4	587.0
SA-0/PA	9.3	14.3
SA-15/PA	309.6	382.7

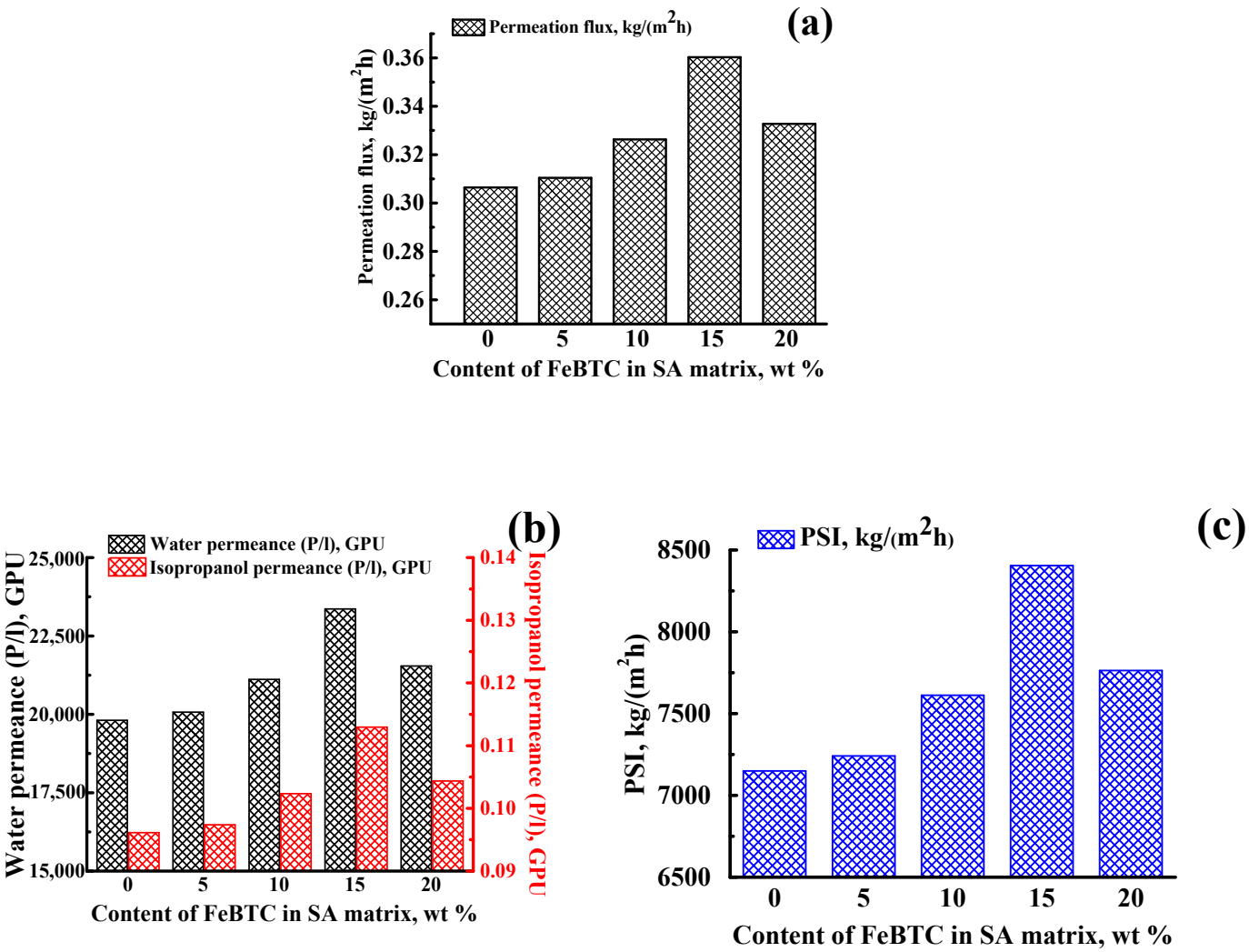

Figure 9. Dependence of the (**a**) permeation flux, (**b**) water and isopropanol permeances and (**c**) PSI on the FeBTC content in the sodium alginate (SA) matrix for the pervaporation of the water/isopropanol (30/70 wt %) mixture at 22 °C. The water content in the permeate for all membranes was 99.99 wt %.

The data presented in Table 3 demonstrate that the membrane cross-linking increases the values of average roughness (Ra) and root mean square roughness (Rq) compared to the SA-0 membrane (Table 2). The introduction of 15 wt % FeBTC and cross-linking by citric acid (SA-15/CA membrane) increases Ra 42.2-fold and Rq 28.5-fold compared to the SA-0/CA membrane, while the introduction of 15 wt % FeBTC and cross-linking with phosphoric acid (SA-15/PA membrane) increases Ra 33.3-fold and Rq 26.8-fold compared to the SA-0/PA membrane. The roughness of the membranes is consistent with the SEM data (Figure 6) and the transport properties of cross-linked SA and SA-FeBTC membranes (Figure 10a). The SA-15/CA membrane has the largest values of surface roughness, causing the highest values of permeation flux among the cross-linked membranes (Figure 10a).

3.1.6. Swelling Degree

The swelling degree was studied in a water–isopropanol mixture (30/70 wt %) and pure water. For the untreated SA and SA-FeBTC membranes, the swelling degree was studied only for the water/isopropanol (30/70 wt %) mixture since these membranes instantly dissolve in pure water. The data are shown in Table 4.

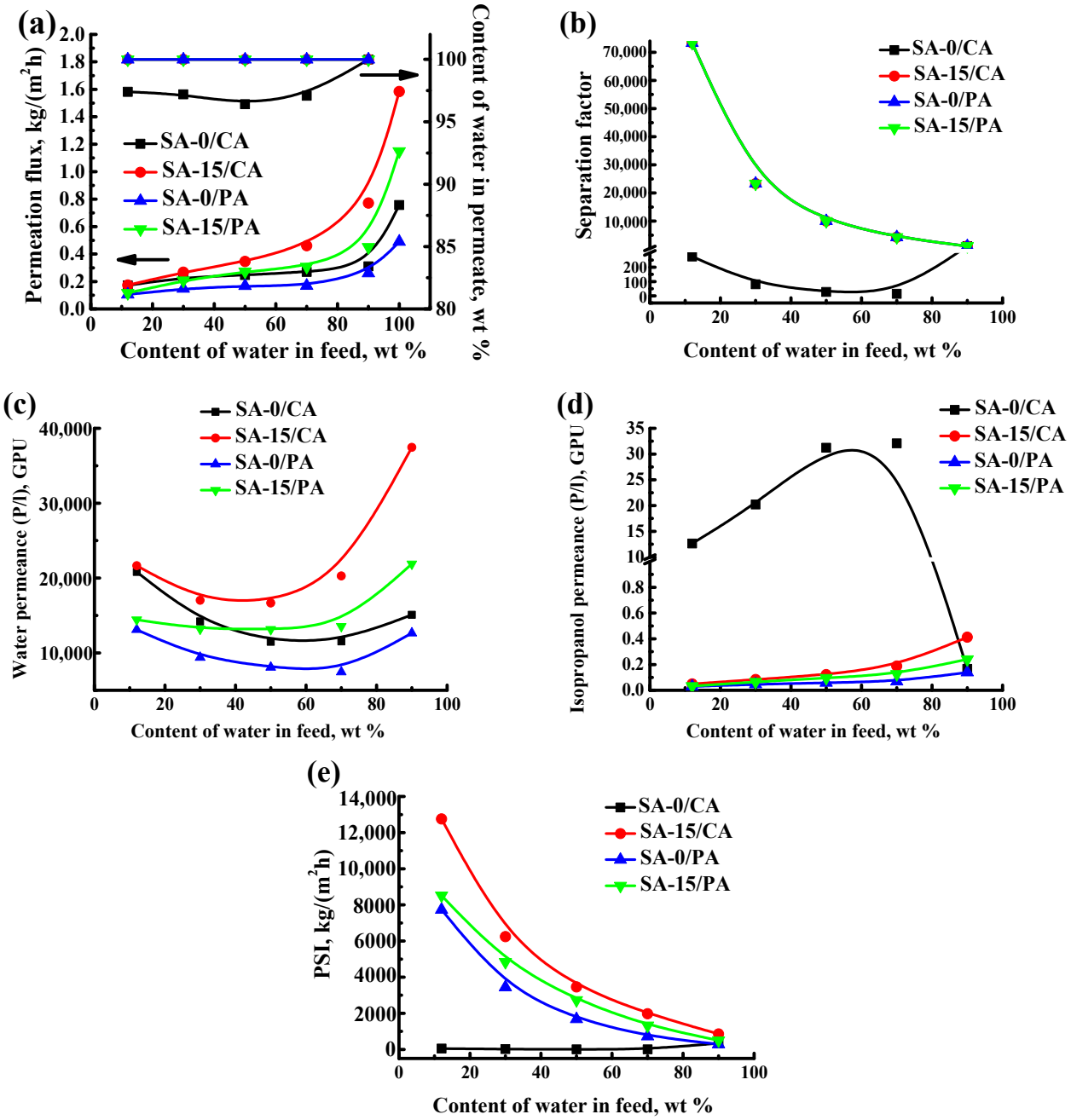

Figure 10. The dependence of (**a**) permeation flux and water content in the permeate, (**b**) separation factor, (**c**) water permeance, (**d**) isopropanol permeance and (**e**) pervaporation separation index (PSI) on the water content in the feed in the pervaporation of the water/isopropanol mixture at 22 °C using cross-linked sodium alginate (SA) and SA-FeBTC membranes.

Table 4. Swelling degree in water/isopropanol mixture and water for the SA and SA-FeBTC membranes.

Membrane	Swelling Degree, %	
	Water/Isopropanol (30/70 wt %)	Water
SA-0	13	–
SA-15	19	–
SA-0/CA	27	120
SA-15/CA	49	166
SA-0/PA	28	85
SA-15/PA	35	99

The data presented in Table 4 demonstrate that the addition of 15 wt % FeBTC (SA-15 membrane) increases the swelling degree in the water–isopropanol mixture compared to the SA-0 membrane, which may be due to the decreased crystallinity degree of the modified SA-15 membrane (confirmed by NMR data, Figure 2). The cross-linking of the SA and SA-FeBTC membranes with acids stabilizes them in water compared to the untreated SA-0 and SA-15 membranes, as the cross-linking of sodium alginate with acids (CA and PA) leads to the robust cross-linking of polymer chains according to the mechanisms described in [37,106]. The SA-0/PA membrane has a lower swelling degree in water (85%) compared to the SA-0/CA membrane (120%). This indicates a greater degree of cross-linking of the polymer chains with PA, resulting in a lower permeability in the pervaporation dehydration of isopropanol (Figure 10a). The data on the swelling degree in the water–isopropanol (30/70 wt %) mixture indicate a change in the structural characteristics during the cross-linking of the membranes. The increased swelling degree for cross-linked SA-0/CA and SA-0/PA membranes compared to the SA-0 membrane may be associated with the formation of a hydrophilic electrolyte complex during the cross-linking and the change in the surface characteristics of the membranes. The introduction of 15 wt % FeBTC and the cross-linking of polymer chains of sodium alginate with acids (CA and PA) increases the swelling degree in both pure water and a water–isopropanol (30/70 wt %) mixture as compared with the uncross-linked SA-15 and cross-linked SA-0/PA and SA-0/CA membranes. This may be related to the porous structure of the modifier FeBTC, selective sorption of water by iron ions and the semi-amorphous nature of the modifier FeBTC. An increase in swelling results in increased permeation flux of the modified membranes (Figures 9 and 10a).

3.2. Transport Properties of SA and SA-FeBTC-Based Membranes

3.2.1. Pervaporation Performance of the Untreated SA and SA-FeBTC Membranes

Pervaporation is most often used not as an independent process, but in hybrid processes, for example, in "pervaporation + distillation," where a mixture containing up to 30 wt % of water often comes out of the distillation column. To study the developed membranes under conditions close to the real, the transport properties of untreated SA-FeBTC membranes were studied in the pervaporation of a water–isopropanol (30/70 wt %) mixture at 22 °C. The dependence of the permeation flux, water content in the permeate, component (water and isopropanol) permeances and PSI on the FeBTC content in the SA matrix is presented in Figure 9.

The developed membranes based on the SA and SA-FeBTC composites are highly selective with respect to water (the water content in the permeate is 99.99 wt %). The permeation flux for the modified SA-FeBTC membranes increased compared to a membrane based on SA. The maximum permeation flux of 0.36 kg/(m^2h) was demonstrated by a membrane containing 15 wt % FeBTC in the SA matrix (SA-15), which is ~18% higher than for a membrane based on pure SA (SA-0). The maximum value of the permeation flux is consistent with the structural and physicochemical properties of the membranes: the increased membrane surface roughness and swelling degree in separated mixture (confirmed by AFM and swelling degree data in Sections 3.1.5 and 3.1.6). The decrease in the permeation flux for the SA-20 membrane is due to the high agglomeration of FeBTC in the SA matrix and on the membrane surface (confirmed by SEM and AFM data in Sections 3.1.4 and 3.1.5), which leads to hindered mass transfer of the feed components through the membrane. Figure 1b shows the dependence of the component (water and isopropanol) permeances and PSI on the FeBTC content in the SA matrix. It was shown that the SA-15 membrane has the highest water permeance and PSI, which demonstrated the efficiency of the separation of the water/isopropanol (30/70 wt %) mixture by this membrane. Thus, 15 wt % FeBTC was chosen as the optimal concentration of the modifier in SA matrix. This membrane was submitted to further cross-linking with acids to achieve membrane stability in diluted isopropanol solutions.

3.2.2. Pervaporation Performance of Cross-Linked SA and SA-FeBTC Membranes

For the use of membranes in a wide concentration range of isopropanol solutions, cross-linked SA and SA-FeBTC (15%) membranes were developed. Polymer chains of SA were cross-linked with phosphoric and citric acids. Transport properties of cross-linked membranes such as permeation flux, water content in permeate, separation factor, component (water and isopropanol) permeances and PSI in the pervaporation of the water/isopropanol mixture at 22 °C are shown in Figure 10.

The data presented in Figure 10 demonstrate that the cross-linking of polymer chains with acids makes it possible to use the developed cross-linked dense membranes in the pervaporation separation of the entire concentration range of a water/isopropanol mixture (12–100 wt % water). The unmodified membrane cross-linked by phosphoric acid (SA-0/PA) has a lower permeation flux compared to the membrane cross-linked by citric acid (SA-0/CA). The more noticeable decrease in the permeation flux in the case of cross-linking with phosphoric acid as compared with citric acid can be related to a stronger (deeper) membrane cross-linking due to protonation of the carboxyl group and the formation of –C–O–P– bonds (confirmed by FTIR and NMR data, Sections 3.1.2 and 3.2.1). In the case of citric acid, only the protonation of the carboxyl group was observed by NMR (Section 3.1.2). At the same time, cross-linking with citric acid led to a decrease in the water content in the permeate (Figure 10a), which was related to the higher swelling degree of this membrane in water compared to the SA-0/PA membrane (confirmed by the swelling degree data, Section 3.1.6). Cross-linking of polymer chains with acids decreased the permeation flux from 0.306 kg/(m^2h) for the unmodified membrane to 0.229 kg/(m^2h) for the cross-linked membrane with citric acid, and to 0.148 kg/(m^2h) for the cross-linked membrane with phosphoric acid due to a decrease in free volume between polymer chains. The introduction of 15 wt % FeBTC increased permeation flux compared with the unmodified cross-linked membranes. It is also worth noting that the SA-15/CA membrane has 27–71% higher permeation flux in the pervaporation of the water/isopropanol (12–100 wt % water) mixture compared to the SA-15/PA membrane (Figure 10a). Figure 10b shows that three membranes (SA-15/CA, SA-0/PA and SA-15/PA) have the same separation factor over the entire concentration range, since the water content in the permeate for these membranes was constant at 99.99 wt %. For the SA-0/CA membrane, the separation factor was lower (water content in the permeate more 96.4 wt %, Figure 10a). Figure 10c,d shows the dependence of the component (water and isopropanol) permeances on the water content in the feed. As it was mentioned in the introduction, the development of the novel membranes was carried out to prevent the permeability/selectivity trade-off. The data in Figure 10 demonstrate that the unmodified cross-linked membranes (SA-0/CA and SA-0/PA) also exhibit the same problem of the balance between permeability and selectivity. However, the introduction of FeBTC in the SA matrix and cross-linking with CA (SA-15/CA membrane) improved the permeation flux and membrane selectivity (constant 99.99 wt % water in the permeate) compared to the SA-0/CA membrane. This may be related to a decrease in isopropanol permeance of the modified membrane compared to the unmodified SA-0/CA membrane. In this case, the window sizes for FeBTC (5.5 and 8.6 Å) were smaller than the isopropanol molecular size (~16 Å [18]), providing a significant retention of isopropanol molecules and selective diffusion of water (with smaller molecular size ~1 Å [107]) through the membrane. The modifier FeBTC also ensured the selective sorption of water by iron ions in the SA-15/CA membrane. The data presented show that the SA-15/CA membrane has the highest water permeance.

Furthermore, to demonstrate the efficiency, the PSI values are presented in Figure 10e, which demonstrates that the curve for SA-15/CA membrane lies higher than for other membranes, which shows the efficiency of the separation of the water–isopropanol mixture by this membrane. Thus, the developed SA-15/CA membrane has the optimal transport characteristics in pervaporation dehydration of isopropanol.

3.3. Comparison of the Performance with SA-Based Membranes Described in the Literature

Transport properties of the cross-linked dense SA-15/CA membrane were compared with the literature data on the SA-based dense membranes applied for pervaporation dehydration of isopropanol (Table 5).

Table 5. Transport properties of the cross-linked dense SA-15/CA membrane and literature data on the SA-based dense membranes applied for pervaporation dehydration of isopropanol.

Membranes	T, °C	Thickness, μm	Water Content in the Feed, wt.%	Permeation Flux, g/(m^{2}h)	Normalized Permeation flux J_n, g/(m^2·h·μm)	Separation Factor (β)	Reference
SA-15/CA	22	25	30	267	10.68	23,331	This study
SA/poly(ε-caprolactone)/6% graphene oxide	30	82	20	~506	~6.17	~73	[108]
SA + 40 wt % TiO_2 (cross-linked)	30	40	25	~286	~7.15	~980	[109]
SA + 5 wt % polyvinyl alcohol	30	30	30	226	7.53	49.5	[28]
SA + 10 wt % SBA-15	30	50	20	333	6.66	∞	[110]
SA + 10 wt % Fe-SBA-15	30	50	20	390	7.8	∞	[110]
SA + 30 wt % NaY	30	40	25	351	8.775	62.15	[111]
SA + 15 wt % gelatin	30	45	25	~236	~5.24	~650	[112]
SA + 10 wt % tetraethyl orthosilicate	30	50	25	~250	~5	~170	[113]
SA+polystyrene sulfonic acid-co-maleic acid	30	40	30	~223	~5.58	~1800	[114]
SA + 2 wt % chitosan-wrapped multiwalled carbon nanotubes	30	50	25	~324	~6.48	590	[16]
SA–heteropolyacids (10 wt %)	30	40	30	~263	~6.58	~1200	[115]
SA + 15 wt % magnesium aluminum silicate	50	50	30	125	2.5	266	[116]
SA + 20 wt % aluminum-containing mesoporous silica	30	60–65	30	256	~4.1	∞	[117]
SA + 5 wt % sodium montmorillonite	30	50	20	102	2.04	∞	[118]
Polyacrylamide-grafted-sodium alginate copolymers (1:1)	30	30	30	325	10.83	36.6	[27]

The data presented in Table 5 demonstrate that the cross-linked SA-15/CA membrane developed in this work has a high separation factor, superior to the majority of dense membranes described in the literature, and a high level of permeation flux and normalized permeation flux (permeation flux divided on membrane thickness). The developed SA-15/CA

membrane is only slightly inferior to the SA + 10 wt % SBA-15, SA + 10 wt % Fe-SBA-15 and SA + 20 wt % aluminum-containing mesoporous silica membranes [110,117]. However, these membranes were tested only up to 20% and 30% water content in the feed [110,117]. At the same time, the developed SA-15/CA membrane was stable and demonstrated high values of permeation flux (174–771 g/(m^2h)) and constant selectivity (99.99 wt % water in the permeate) in the pervaporation dehydration of isopropanol in a wide concentration range (12–90 wt % water). In order to increase the permeation flux maintaining a high selectivity, in further studies, supported membranes cross-linked with CA will be developed by reducing the thickness of the selective layer based on the SA-15%FeBTC composite, deposited on a porous substrate.

4. Conclusions

In the present study, novel dense mixed matrix membranes based on biopolymer SA modified with FeBTC were developed and tested. The studies were undertaken to improve the pervaporation dehydration properties of a parent SA membrane. The improvement of the transport properties of modified dense SA membranes was related to FeBTC porous structure, its excellent stability in the water–organic solvent system, and hydrophobic/hydrophilic properties. The effective modification led to a change in the free volume, membrane morphology, increase of the swelling degree and surface roughness of the polymer membranes. It was shown that the optimum FeBTC content in the SA matrix was 15 wt %, which led to an increase in permeation flux compared to the untreated membranes at high water content in the permeate (99.99 wt %) in pervaporation dehydration of isopropanol (30 wt % water). A further increase in the content of FeBTC decreased the permeation flux due to the agglomeration of particles.

Two types of cross-linking of SA polymer chains have been developed, treated with citric or phosphoric acid. It was shown that the cross-linking of the polymer chains stabilized the developed membranes in water and dilute solutions (confirmed by the swelling data). The cross-linking of SA polymer chains decreased the permeation flux in the pervaporation dehydration of isopropanol (30 wt % water) compared to the untreated SA-0 membrane, which could be caused by a decrease in free volume (the cross-linking of polymer chains was proven using FTIR and NMR). It was shown that the introduction of 15 wt % FeBTC into SA and cross-linking with acids led to significant changes in the inner and surface structure of membranes, and higher thermal stability compared to the unmodified cross-linked SA membranes, which was studied by SEM, AFM and TGA.

To conclude, an SA-based membrane modified by 15 wt % FeBTC and cross-linked with citric acid exhibited optimal transport properties for the pervaporation of a water–isopropanol mixture (12–100 wt % water): 174–1584 g/(m^2h) permeation flux and constant 99.99 wt % water content in permeate.

Author Contributions: Conceptualization, A.K. and A.P.; methodology, A.K. and A.P.; analysis, A.K. and A.P.; investigation, A.K., M.D., S.E. and A.M.; resources, A.P.; data curation, A.K. and A.P.; writing—original draft preparation, A.K.; writing—review and editing, A.K., M.D. and A.P.; visualization, A.K. and A.P.; supervision, A.P.; project administration, A.P.; funding acquisition, A.P. All authors have read and agreed to the published version of the manuscript.

Funding: The reported study was funded by RFBR, project number 19-38-90008.

Institutional Review Board Statement: Not applicable.

Informed Consent Statement: Not applicable.

Data Availability Statement: Not applicable.

Acknowledgments: The experimental work of this study was facilitated by the equipment from the Resource Centre of Geomodel, Chemical Analysis and Materials Research Centre, Centre for X-ray Diffraction Methods, Magnetic Resonance Research Centre, Centre for Innovative Technologies of Composite Nanomaterials, Nanophotonics Centre, Cryogenic department, Thermogravimetric and

Calorimetric Research Centre and the Interdisciplinary Resource Centre for Nanotechnology at the St. Petersburg State University.

Conflicts of Interest: The authors declare no conflict of interest.

References

1. Atlaskin, A.A.; Trubyanov, M.M.; Yanbikov, N.R.; Bukovsky, M.V.; Drozdov, P.N.; Vorotyntsev, V.M.; Vorotyntsev, I.V. Total Reflux Operating Mode of Apparatuses of a Membrane Column Type during High Purification of Gases to Remove a Highly Permeable Impurity. *Pet. Chem.* **2018**, *58*, 508–517. [CrossRef]
2. Atlaskin, A.A.; Trubyanov, M.M.; Yanbikov, N.R.; Vorotyntsev, A.V.; Drozdov, P.N.; Vorotyntsev, V.M.; Vorotyntsev, I.V. Comprehensive experimental study of membrane cascades type of "continuous membrane column" for gases high-purification. *J. Membr. Sci.* **2019**, *572*, 92–101. [CrossRef]
3. Davletbaeva, I.M.; Zaripov, I.I.; Mazilnikov, A.I.; Davletbaev, R.S.; Sharifullin, R.R.; Atlaskin, A.A.; Sazanova, T.S.; Vorotyntsev, I.V. Synthesis and Study of Gas Transport Properties of Polymers Based on Macroinitiators and 2,4-Toluene Diisocyanate. *Membranes* **2019**, *9*, 42. [CrossRef] [PubMed]
4. Besha, A.T.; Tsehaye, M.T.; Tiruye, G.A.; Gebreyohannes, A.Y.; Awoke, A.; Tufa, R.A. Deployable Membrane-Based Energy Technologies: The Ethiopian Prospect. *Sustainability* **2020**, *12*, 8792. [CrossRef]
5. Gui, S.; Mai, Z.; Fu, J.; Wei, Y.; Wan, J. Transport Models of Ammonium Nitrogen in Wastewater from Rare Earth Smelteries by Reverse Osmosis Membranes. *Sustainability* **2020**, *12*, 6230. [CrossRef]
6. Yushkin, A.A.; Golubev, G.S.; Podtynnikov, I.A.; Borisov, I.L.; Volkov, V.V. Separation of Mixtures of Polar and Nonpolar Organic Liquids by Pervaporation and Nanofiltration (Review). *Pet. Chem.* **2020**, *60*, 1317–1327. [CrossRef]
7. Apel, P.Y.; Bobreshova, O.V.; Volkov, A.V.; Nikonenko, V.V.; Stenina, I.A.; Filippov, A.N.; Yampolskii, Y.P.; Yaroslavtsev, A.B. Prospects of Membrane Science Development. *Membr. Membr. Technol.* **2019**, *1*, 45–63. [CrossRef]
8. Ogorodnikov, S.K.; Lesteva, T.M.; Kogan, V.B. *Azeotrope Mixtures*; Chemistry: St. Petersburg, Russia, 1971.
9. Lin, F.; Zhang, S.; Ma, G.; Qiu, L.; Sun, H. Application of Ceramic Membrane in Water and Wastewater Treatment. *E3S Web Conf.* **2018**, *53*, 04032. [CrossRef]
10. Achiou, B.; Beqqour, D.; Elomari, H.; Bouazizi, A.; Ouammou, M.; Bouhria, M.; Aaddane, A.; Khiat, K.; Younssi, S.A. Preparation of inexpensive NaA zeolite membrane on pozzolan support at low temperature for dehydration of alcohol solutions. *J. Environ. Chem. Eng.* **2018**, *6*, 4429–4437. [CrossRef]
11. Klinov, A.V.; Akberov, R.R.; Fazlyev, A.R.; Farakhov, M.I. Experimental investigation and modeling through using the solution-diffusion concept of pervaporation dehydration of ethanol and isopropanol by ceramic membranes HybSi. *J. Membr. Sci.* **2017**, *524*, 321–333. [CrossRef]
12. Dmitrenko, M.; Penkova, A.; Kuzminova, A.; Morshed, M.; Larionov, M.; Alem, H.; Zolotarev, A.; Ermakov, S.; Roizard, D. Investigation of new modification strategies for PVA membranes to improve their dehydration properties by pervaporation. *Appl. Surf. Sci.* **2018**, *450*, 527–537. [CrossRef]
13. Benzaqui, M.; Semino, R.; Carn, F.; Tavares, S.R.; Menguy, N.; Giménez-Marqués, M.; Bellido, E.; Horcajada, P.; Berthelot, T.; Kuzminova, A.I.; et al. Covalent and Selective Grafting of Polyethylene Glycol Brushes at the Surface of ZIF-8 for the Processing of Membranes for Pervaporation. *ACS Sustain. Chem. Eng.* **2019**, *7*, 6629–6639. [CrossRef]
14. Dmitrenko, M.; Liamin, V.; Kuzminova, A.; Mazur, A.; Lahderanta, E.; Ermakov, S.; Penkova, A. Novel Mixed Matrix Sodium Alginate–Fullerenol Membranes: Development, Characterization, and Study in Pervaporation Dehydration of Isopropanol. *Polymers* **2020**, *12*, 864. [CrossRef]
15. Toti, U.S.; Aminabhavi, T.M. Pervaporation separation of water-isopropyl alcohol mixtures with blend membranes of sodium alginate and poly(acrylamide)-grafted guar gum. *J. Appl. Polym. Sci.* **2002**, *85*, 2014–2024. [CrossRef]
16. Sajjan, A.; Kumar, B.J.; Kittur, A.; Kariduraganavar, M. Novel approach for the development of pervaporation membranes using sodium alginate and chitosan-wrapped multiwalled carbon nanotubes for the dehydration of isopropanol. *J. Membr. Sci.* **2013**, *425–426*, 77–88. [CrossRef]
17. Dmitrenko, M.; Liamin, V.; Lahderanta, E.; Ermakov, S.; Penkova, A. Mixed matrix membranes based on sodium alginate modified by fullerene derivatives with L-amino acids for pervaporation isopropanol dehydration. *J. Mater. Sci.* **2021**, *56*, 7765–7787. [CrossRef]
18. Kuzminova, A.I.; Dmitrenko, M.E.; Poloneeva, D.Y.; Selyutin, A.A.; Mazur, A.S.; Emeline, A.V.; Mikhailovskii, V.Y.; Solovyev, N.D.; Ermakov, S.S.; Penkova, A.V. Sustainable composite pervaporation membranes based on sodium alginate modified by metal organic frameworks for dehydration of isopropanol. *J. Membr. Sci.* **2021**, *626*, 119194. [CrossRef]
19. Chaudhari, S.; Baek, M.; Kwon, Y.; Shon, M.; Nam, S.; Park, Y. Surface-modified halloysite nanotube-embedded polyvinyl alcohol/polyvinyl amine blended membranes for pervaporation dehydration of water/isopropanol mixtures. *Appl. Surf. Sci.* **2019**, *493*, 193–201. [CrossRef]
20. Rao, K.S.V.K.; Subha, M.C.S.; Sairam, M.; Mallikarjuna, N.N.; Aminabhavi, T.M. Blend membranes of chitosan and poly(vinyl alcohol) in pervaporation dehydration of isopropanol and tetrahydrofuran. *J. Appl. Polym. Sci.* **2006**, *103*, 1918–1926. [CrossRef]
21. Zhang, W.; Li, G.; Fang, Y.; Wang, X. Maleic anhydride surface-modification of crosslinked chitosan membrane and its pervaporation performance. *J. Membr. Sci.* **2007**, *295*, 130–138. [CrossRef]

22. Ge, J.; Cui, Y.; Yan, Y.; Jiang, W. The effect of structure on pervaporation of chitosan membrane. *J. Membr. Sci.* **2000**, *165*, 75–81. [CrossRef]
23. Tang, S.; Dong, Z.; Zhu, X.; Zhao, Q. A poly (ionic liquid) complex membrane for pervaporation dehydration of acidic water-isopropanol mixtures. *J. Membr. Sci.* **2019**, *576*, 59–65. [CrossRef]
24. Van Baelen, D.; Van der Bruggen, B.; Dungen, K.V.D.; Degreve, J.; Vandecasteele, C. Pervaporation of water–alcohol mixtures and acetic acid–water mixtures. *Chem. Eng. Sci.* **2005**, *60*, 1583–1590. [CrossRef]
25. Albo, J.; Wang, J.; Tsuru, T. Application of interfacially polymerized polyamide composite membranes to isopropanol dehydration: Effect of membrane pre-treatment and temperature. *J. Membr. Sci.* **2014**, *453*, 384–393. [CrossRef]
26. Smuleac, V.; Wu, J.; Nemser, S.; Majumdar, S.; Bhattacharyya, D. Novel perfluorinated polymer-based pervaporation membranes for the separation of solvent/water mixtures. *J. Membr. Sci.* **2010**, *352*, 41–49. [CrossRef] [PubMed]
27. Toti, U.S.; Aminabhavi, T.M. Synthesis and characterization of polyacrylamidegrafted sodium alginate membranes for pervaporation separation of water + isopropanol mixtures. *J. Appl. Polym. Sci.* **2004**, *92*, 2030–2037. [CrossRef]
28. Toti, U.S.; Aminabhavi, T.M. Different viscosity grade sodium alginate and modified sodium alginate membranes in pervaporation separation of water + acetic acid and water + isopropanol mixtures. *J. Membr. Sci.* **2004**, *228*, 199–208. [CrossRef]
29. Ho, B.; Azahari, B.; Yhaya, M.; Talebi, A.; Ng, C.; Tajarudin, H.; Ismail, N. Green Technology Approach for Reinforcement of Calcium Chloride Cured Sodium Alginate Films by Isolated Bacteria from Palm Oil Mill Effluent (POME). *Sustainability* **2020**, *12*, 9468. [CrossRef]
30. Jung, J.; Hu, J.W. Characterization of Polyethylene Oxide and Sodium Alginate for Oil Contaminated-Sand Remediation. *Sustainability* **2017**, *9*, 62. [CrossRef]
31. Yakoumis, I.; Theodorakopoulos, G.; Papageorgiou, S.K.; Romanos, G.; Veziri, C.; Panias, D. Tubular C/Cu decorated γ-alumina membranes for NO abatement. *J. Membr. Sci.* **2016**, *515*, 134–143. [CrossRef]
32. Kuila, S.B.; Ray, S.K. Dehydration of dioxane by pervaporation using filled blend membranes of polyvinyl alcohol and sodium alginate. *Carbohydr. Polym.* **2014**, *101*, 1154–1165. [CrossRef]
33. Moulik, S.; Nazia, S.; Vani, B.; Sridhar, S. Pervaporation separation of acetic acid/water mixtures through sodium alginate/polyaniline polyion complex membrane. *Sep. Purif. Technol.* **2016**, *170*, 30–39. [CrossRef]
34. Hosseini, S.; Charkhi, A.; Minuchehr, A.; Ahmadi, S.J. Dehydration of acetonitrile using cross-linked sodium alginate membrane containing nano-sized NaA zeolite. *Chem. Pap.* **2017**, *71*, 1143–1153. [CrossRef]
35. Xing, R.; Pan, F.; Zhao, J.; Cao, K.; Gao, C.; Yang, S.; Liu, G.; Wu, H.; Jiang, Z. Enhancing the permeation selectivity of sodium alginate membrane by incorporating attapulgite nanorods for ethanol dehydration. *RSC Adv.* **2016**, *6*, 14381–14392. [CrossRef]
36. Cheng, X.; Jiang, Z.; Cheng, X.; Yang, H.; Tang, L.; Liu, G.; Wang, M.; Wu, H.; Pan, F.; Cao, X. Water-selective permeation in hybrid membrane incorporating multi-functional hollow ZIF-8 nanospheres. *J. Membr. Sci.* **2018**, *555*, 146–156. [CrossRef]
37. Kalyani, S.; Smitha, B.; Sridhar, S.; Krishnaiah, A. Pervaporation separation of ethanol–water mixtures through sodium alginate membranes. *Desalination* **2008**, *229*, 68–81. [CrossRef]
38. Dong, Y.; Zhang, L.; Shen, J.; Song, M.; Chen, H. Preparation of poly (vinyl alcohol)-sodium alginate hollow-fiber composite membranes and pervaporation dehydration characterization of aqueous alcohol mixtures. *Desalination* **2006**, *193*, 202–210. [CrossRef]
39. Zhao, F.-Y.; An, Q.-F.; Ji, Y.-L.; Gao, C.-J. A novel type of polyelectrolyte complex/MWCNT hybrid nanofiltration membranes for water softening. *J. Membr. Sci.* **2015**, *492*, 412–421. [CrossRef]
40. Aburabie, J.H.; Puspasari, T.; Peinemann, K.-V. Alginate-based membranes: Paving the way for green organic solvent nanofiltration. *J. Membr. Sci.* **2020**, *596*, 117615. [CrossRef]
41. Zhao, X.; Qin, A.; Liu, D.; He, C. Tuning the antifouling property of PVDF ultrafiltration membrane with surface anchored polyelectrolyte complexes for sewage treatment. *RSC Adv.* **2015**, *5*, 63580–63587. [CrossRef]
42. Li, J.; Si, X.; Li, X.; Wang, N.; An, Q.; Ji, S. Preparation of acid-resistant PEI/SA composite membranes for the pervaporation dehydration of ethanol at low pH. *Sep. Purif. Technol.* **2018**, *192*, 205–212. [CrossRef]
43. Liu, G.; Jiang, Z.; Cheng, X.; Chen, C.; Yang, H.; Wu, H.; Pan, F.; Zhang, P.; Cao, X. Elevating the selectivity of layer-by-layer membranes by in situ bioinspired mineralization. *J. Membr. Sci.* **2016**, *520*, 364–373. [CrossRef]
44. Saraswathi, M.; Rao, K.M.; Prabhakar, M.; Prasad, C.; Sudakar, K.; Kumar, H.N.; Prasad, M.; Rao, K.C.; Subha, M. Pervaporation studies of sodium alginate (SA)/dextrin blend membranes for separation of water and isopropanol mixture. *Desalination* **2011**, *269*, 177–183. [CrossRef]
45. Dudek, G.; Turczyn, R.; Gnus, M.; Konieczny, K. Pervaporative dehydration of ethanol/water mixture through hybrid alginate membranes with ferroferic oxide nanoparticles. *Sep. Purif. Technol.* **2018**, *193*, 398–407. [CrossRef]
46. Zhao, C.; Jiang, Z.; Zhao, J.; Cao, K.; Zhang, Q.; Pan, F. High Pervaporation Dehydration Performance of the Composite Membrane with an Ultrathin Alginate/Poly (acrylic acid)–Fe_3O_4 Active Layer. *Ind. Eng. Chem. Res.* **2014**, *53*, 1606–1616. [CrossRef]
47. Dudek, G.; Krasowska, M.; Turczyn, R.; Strzelewicz, A.; Djurado, D.; Pouget, S. Clustering analysis for pervaporation performance assessment of alginate hybrid membranes in dehydration of ethanol. *Chem. Eng. Res. Des.* **2019**, *144*, 483–493. [CrossRef]
48. Dudek, G.; Krasowska, M.; Turczyn, R.; Gnus, M.; Strzelewicz, A. Structure, morphology and separation efficiency of hybrid Alg/Fe_3O_4 membranes in pervaporative dehydration of ethanol. *Sep. Purif. Technol.* **2017**, *182*, 101–109. [CrossRef]
49. Ji, C.-H.; Xue, S.-M.; Xu, Z.-L. Novel Swelling-Resistant Sodium Alginate Membrane Branching Modified by Glycogen for Highly Aqueous Ethanol Solution Pervaporation. *ACS Appl. Mater. Interfaces* **2016**, *8*, 27243–27253. [CrossRef]

50. Nigiz, F.U. Graphene oxide-sodium alginate membrane for seawater desalination through pervaporation. *Desalination* **2020**, *485*, 114465. [CrossRef]
51. Yang, H.; Wu, H.; Pan, F.; Li, Z.; Ding, H.; Liu, G.; Jiang, Z.; Zhang, P.; Cao, X.; Wang, B. Highly water-permeable and stable hybrid membrane with asymmetric covalent organic framework distribution. *J. Membr. Sci.* **2016**, *520*, 583–595. [CrossRef]
52. Yang, H.; Cheng, X.; Cheng, X.; Pan, F.; Wu, H.; Liu, G.; Song, Y.; Cao, X.; Jiang, Z. Highly water-selective membranes based on hollow covalent organic frameworks with fast transport pathways. *J. Membr. Sci.* **2018**, *565*, 331–341. [CrossRef]
53. Nigiz, F.U.; Hilmioglu, N.D. Pervaporation of ethanol/water mixtures by zeolite filled sodium alginate membrane. *Desalination Water Treat.* **2012**, *51*, 637–643. [CrossRef]
54. Su, Z.; Chen, J.H.; Sun, X.; Huang, Y.; Dong, X. Amine-functionalized metal organic framework (NH_2-MIL-125(Ti)) incorporated sodium alginate mixed matrix membranes for dehydration of acetic acid by pervaporation. *RSC Adv.* **2015**, *5*, 99008–99017. [CrossRef]
55. Gao, B.; Jiang, Z.; Zhao, M.; Wu, H.; Pan, F.; Mayta, J.Q.; Chang, Z.; Bu, X. Enhanced dehydration performance of hybrid membranes by incorporating lanthanide-based MOFs. *J. Membr. Sci.* **2018**, *546*, 31–40. [CrossRef]
56. Liu, G.; Jiang, Z.; Cao, K.; Nair, S.; Cheng, X.; Zhao, J.; Gomaa, H.; Wu, H.; Pan, F. Pervaporation performance comparison of hybrid membranes filled with two-dimensional ZIF-L nanosheets and zero-dimensional ZIF-8 nanoparticles. *J. Membr. Sci.* **2017**, *523*, 185–196. [CrossRef]
57. Cheng, X.; Jiang, Z.; Cheng, X.; Guo, S.; Tang, L.; Yang, H.; Wu, H.; Pan, F.; Zhang, P.; Cao, X.; et al. Bimetallic metal-organic frameworks nanocages as multi-functional fillers for water-selective membranes. *J. Membr. Sci.* **2018**, *545*, 19–28. [CrossRef]
58. Jia, Z.; Wu, G. Metal-organic frameworks based mixed matrix membranes for pervaporation. *Microporous Mesoporous Mater.* **2016**, *235*, 151–159. [CrossRef]
59. Ren, Z.; Luo, J.; Wan, Y. Highly permeable biocatalytic membrane prepared by 3D modification: Metal-organic frameworks ameliorate its stability for micropollutants removal. *Chem. Eng. J.* **2018**, *348*, 389–398. [CrossRef]
60. Ren, Y.; Li, T.; Zhang, W.; Wang, S.; Shi, M.; Shan, C.; Zhang, W.; Guan, X.; Lv, L.; Hua, M.; et al. MIL-PVDF blend ultrafiltration membranes with ultrahigh MOF loading for simultaneous adsorption and catalytic oxidation of methylene blue. *J. Hazard. Mater.* **2019**, *365*, 312–321. [CrossRef] [PubMed]
61. Abdullah, N.; Rahman, M.A.; Othman, M.H.D.; Jaafar, J.; Aziz, A.A. Preparation, characterizations and performance evaluations of alumina hollow fiber membrane incorporated with UiO-66 particles for humic acid removal. *J. Membr. Sci.* **2018**, *563*, 162–174. [CrossRef]
62. Lee, J.-Y.; Tang, C.Y.; Huo, F. Fabrication of Porous Matrix Membrane (PMM) Using Metal-Organic Framework as Green Template for Water Treatment. *Sci. Rep.* **2014**, *4*, 3740. [CrossRef]
63. Li, T.; Zhang, W.; Zhai, S.; Gao, G.; Ding, J.; Zhang, W.; Liu, Y.; Zhao, X.; Pan, B.; Lv, L. Efficient removal of nickel (II) from high salinity wastewater by a novel PAA/ZIF-8/PVDF hybrid ultrafiltration membrane. *Water Res.* **2018**, *143*, 87–98. [CrossRef] [PubMed]
64. Cheng, X.; Jiang, X.; Zhang, Y.; Lau, C.H.; Xie, Z.; Ng, D.; Smith, S.J.D.; Hill, M.R.; Shao, L. Building Additional Passageways in Polyamide Membranes with Hydrostable Metal Organic Frameworks to Recycle and Remove Organic Solutes from Various Solvents. *ACS Appl. Mater. Interfaces* **2017**, *9*, 38877–38886. [CrossRef] [PubMed]
65. Gnanasekaran, G.; Balaguru, S.; Arthanareeswaran, G.; Das, D.B. Removal of hazardous material from wastewater by using metal organic framework (MOF) embedded polymeric membranes. *Sep. Sci. Technol.* **2018**, *54*, 434–446. [CrossRef]
66. Liao, Z.; Fang, X.; Xie, J.; Li, Q.; Wang, D.; Sun, X.; Wang, L.; Li, J. Hydrophilic Hollow Nanocube-Functionalized Thin Film Nanocomposite Membrane with Enhanced Nanofiltration Performance. *ACS Appl. Mater. Interfaces* **2019**, *11*, 5344–5352. [CrossRef]
67. Efome, J.E.; Rana, D.; Matsuura, T.; Lan, C.Q. Insight Studies on Metal-Organic Framework Nanofibrous Membrane Adsorption and Activation for Heavy Metal Ions Removal from Aqueous Solution. *ACS Appl. Mater. Interfaces* **2018**, *10*, 18619–18629. [CrossRef] [PubMed]
68. He, Y.; Tang, Y.P.; Ma, D.; Chung, T.-S. UiO-66 incorporated thin-film nanocomposite membranes for efficient selenium and arsenic removal. *J. Membr. Sci.* **2017**, *541*, 262–270. [CrossRef]
69. Gong, X.-Y.; Huang, Z.-H.; Zhang, H.; Liu, W.-L.; Ma, X.-H.; Xu, Z.-L.; Tang, C.Y. Novel high-flux positively charged composite membrane incorporating titanium-based MOFs for heavy metal removal. *Chem. Eng. J.* **2020**, *398*, 125706. [CrossRef]
70. Saleem, H.; Zaidi, S.J. Nanoparticles in reverse osmosis membranes for desalination: A state of the art review. *Desalination* **2020**, *475*, 114171. [CrossRef]
71. Mao, H.; Zhen, H.-G.; Ahmad, A.; Li, S.-H.; Liang, Y.; Ding, J.-F.; Wu, Y.; Li, L.-Z.; Zhao, Z.-P. Highly selective and robust PDMS mixed matrix membranes by embedding two-dimensional ZIF-L for alcohol permselective pervaporation. *J. Membr. Sci.* **2019**, *582*, 307–321. [CrossRef]
72. Han, X.; Sun, H.; Liu, L.; Wang, Y.; He, G.; Li, J. Improved desulfurization performance of polydimethylsiloxane membrane by incorporating metal organic framework CPO-27-Ni. *Sep. Purif. Technol.* **2019**, *217*, 86–94. [CrossRef]
73. Mao, H.; Zhen, H.-G.; Ahmad, A.; Zhang, A.-S.; Zhao, Z.-P. In situ fabrication of MOF nanoparticles in PDMS membrane via interfacial synthesis for enhanced ethanol permselective pervaporation. *J. Membr. Sci.* **2019**, *573*, 344–358. [CrossRef]
74. Khan, A.; Ali, M.; Ilyas, A.; Naik, P.; Vankelecom, I.F.; Gilani, M.A.; Bilad, M.R.; Sajjad, Z.; Khan, A.L. ZIF-67 filled PDMS mixed matrix membranes for recovery of ethanol via pervaporation. *Sep. Purif. Technol.* **2018**, *206*, 50–58. [CrossRef]

75. Li, Q.; Cheng, L.; Shen, J.; Shi, J.; Chen, G.; Zhao, J.; Duan, J.; Liu, G.; Jin, W. Improved ethanol recovery through mixed-matrix membrane with hydrophobic MAF-6 as filler. *Sep. Purif. Technol.* **2017**, *178*, 105–112. [CrossRef]
76. Jin, H.; Liu, X.; Ban, Y.; Peng, Y.; Jiao, W.; Wang, P.; Guo, A.; Li, Y.; Yang, W. Conversion of xylose into furfural in a MOF-based mixed matrix membrane reactor. *Chem. Eng. J.* **2016**, *305*, 12–18. [CrossRef]
77. Zhang, G.; Li, J.; Wang, N.; Fan, H.; Zhang, R.; Ji, S. Enhanced flux of polydimethylsiloxane membrane for ethanol permselective pervaporation via incorporation of MIL-53 particles. *J. Membr. Sci.* **2015**, *492*, 322–330. [CrossRef]
78. Wee, L.H.; Li, Y.; Zhang, K.; Davit, P.; Bordiga, S.; Jiang, J.; Vankelecom, I.F.J.; Martens, J.A. Submicrometer-Sized ZIF-71 Filled Organophilic Membranes for Improved Bioethanol Recovery: Mechanistic Insights by Monte Carlo Simulation and FTIR Spectroscopy. *Adv. Funct. Mater.* **2014**, *25*, 516–525. [CrossRef]
79. De La Iglesia, Ó.; Sorribas, S.; Almendro, E.; Zornoza, B.; Téllez, C.; Coronas, J.; Pedraza, O.D.L.I.; Ariso, C.T. Metal-organic framework MIL-101 (Cr) based mixed matrix membranes for esterification of ethanol and acetic acid in a membrane reactor. *Renew. Energy* **2016**, *88*, 12–19. [CrossRef]
80. Sorribas, S.; Kudasheva, A.; Almendro, E.; Zornoza, B.; de la Iglesia, Ó.; Téllez, C.; Coronas, J. Pervaporation and membrane reactor performance of polyimide based mixed matrix membranes containing MOF HKUST-1. *Chem. Eng. Sci.* **2015**, *124*, 37–44. [CrossRef]
81. Liu, S.; Liu, G.; Shen, J.; Jin, W. Fabrication of MOFs/PEBA mixed matrix membranes and their application in bio-butanol production. *Sep. Purif. Technol.* **2014**, *133*, 40–47. [CrossRef]
82. Han, G.L.; Zhou, K.; Lai, A.N.; Zhang, Q.G.; Zhu, A.M.; Liu, Q.L. $[Cu_2(bdc)_2(bpy)]_n$/SPES-C mixed matrix membranes for separation of methanol/methyl tert-butyl ether mixtures. *J. Membr. Sci.* **2014**, *454*, 36–43. [CrossRef]
83. Vinu, M.; Pal, S.; Chen, J.; Lin, Y.; Lai, Y.; Lee, C.; Lin, C. Microporous 3D aluminum MOF doped into chitosan-based mixed matrix membranes for ethanol/water separation. *J. Chin. Chem. Soc.* **2019**, *66*, 1165–1171. [CrossRef]
84. Vinu, M.; Raja, D.S.; Jiang, Y.-C.; Liu, T.-Y.; Xie, Y.-Y.; Lin, Y.-F.; Yang, C.-C.; Lin, C.-H.; Alshehri, S.M.; Ahamad, T.; et al. Effects of structural crystallinity and defects in microporous Al-MOF filled chitosan mixed matrix membranes for pervaporation of water/ethanol mixtures. *J. Taiwan Inst. Chem. Eng.* **2018**, *83*, 143–151. [CrossRef]
85. Wu, G.; Li, Y.; Geng, Y.; Lu, X.; Jia, Z. Adjustable pervaporation performance of Zr-MOF/poly (vinyl alcohol) mixed matrix membranes. *J. Chem. Technol. Biotechnol.* **2019**, *94*, 973–981. [CrossRef]
86. Zhang, W.; Ying, Y.; Ma, J.; Guo, X.; Huang, H.; Liu, D.; Zhong, C. Mixed matrix membranes incorporated with polydopamine-coated metal-organic framework for dehydration of ethylene glycol by pervaporation. *J. Membr. Sci.* **2017**, *527*, 8–17. [CrossRef]
87. Wu, G.; Jiang, M.; Zhang, T.; Jia, Z. Tunable Pervaporation Performance of Modified MIL-53(Al)-NH_2/Poly (vinyl Alcohol) Mixed Matrix Membranes. *J. Membr. Sci.* **2016**, *507*, 72–80. [CrossRef]
88. Zhang, Y.; Wang, N.; Ji, S.; Zhang, R.; Zhao, C.; Li, J.-R. Metal–organic framework/poly (vinyl alcohol) nanohybrid membrane for the pervaporation of toluene/*n*-heptane mixtures. *J. Membr. Sci.* **2015**, *489*, 144–152. [CrossRef]
89. Wang, H.; Tang, S.; Ni, Y.; Zhang, C.; Zhu, X.; Zhao, Q. Covalent cross-linking for interface engineering of high flux UiO-66-TMS/PDMS pervaporation membranes. *J. Membr. Sci.* **2020**, *598*, 117791. [CrossRef]
90. Mao, H.; Li, S.-H.; Zhang, A.-S.; Xu, L.-H.; Lu, J.-J.; Zhao, Z.-P. Novel MOF-capped halloysite nanotubes/PDMS mixed matrix membranes for enhanced *n*-butanol permselective pervaporation. *J. Membr. Sci.* **2020**, *595*, 117543. [CrossRef]
91. Zhang, X.; Cheng, F.-Y.; Zhang, H.-Z.; Xu, Z.-L.; Xue, S.-M.; Ma, X.-H.; Xu, X.-R. In-situ synthetic modified metal-organic framework (MZIF-8) as an interlayer of the composite membranes for ethanol dehydration. *J. Membr. Sci.* **2020**, *601*, 117916. [CrossRef]
92. Li, Q.; Liu, Q.; Zhao, J.; Hua, Y.; Sun, J.; Duan, J.; Jin, W. High efficient water/ethanol separation by a mixed matrix membrane incorporating MOF filler with high water adsorption capacity. *J. Membr. Sci.* **2017**, *544*, 68–78. [CrossRef]
93. Gao, R.; Zhang, Q.; Lv, R.; Soyekwo, F.; Zhu, A.; Liu, Q. Highly efficient polymer–MOF nanocomposite membrane for pervaporation separation of water/methanol/MTBE ternary mixture. *Chem. Eng. Res. Des.* **2017**, *117*, 688–697. [CrossRef]
94. Wang, N.; Zhang, G.; Wang, L.; Li, J.; An, Q.; Ji, S. Pervaporation dehydration of acetic acid using NH 2 -UiO-66/PEI mixed matrix membranes. *Sep. Purif. Technol.* **2017**, *186*, 20–27. [CrossRef]
95. Gascón, V.; Jiménez, M.B.; Blanco, R.M.; Sanchez-Sanchez, M. Semi-crystalline Fe-BTC MOF material as an efficient support for enzyme immobilization. *Catal. Today* **2018**, *304*, 119–126. [CrossRef]
96. Hu, X.; Lou, X.; Li, C.; Ning, Y.; Liao, Y.; Chen, Q.; Mananga, E.S.; Shen, M.; Hu, B. Facile synthesis of the Basolite F300-like nanoscale Fe-BTC framework and its lithium storage properties. *RSC Adv.* **2016**, *6*, 114483–114490. [CrossRef]
97. Shi, J.; Hei, S.; Liu, H.; Fu, Y.; Zhang, F.; Zhong, Y.; Zhu, W. Synthesis of MIL-100 (Fe) at Low Temperature and Atmospheric Pressure. *J. Chem.* **2013**, *2013*, 792827. [CrossRef]
98. Fu, Y.-Y.; Yang, C.-X.; Yan, X.-P. Metal-organic framework MIL-100 (Fe) as the stationary phase for both normal-phase and reverse-phase high performance liquid chromatography. *J. Chromatogr. A* **2013**, *1274*, 137–144. [CrossRef] [PubMed]
99. Msahel, A.; Galiano, F.; Pilloni, M.; Russo, F.; Hafiane, A.; Castro-Muñoz, R.; Kumar, V.; Gedanken, A.; Ennas, G.; Porat, Z.; et al. Exploring the Effect of Iron Metal-Organic Framework Particles in Polylactic Acid Membranes for the Azeotropic Separation of Organic/Organic Mixtures by Pervaporation. *Membranes* **2021**, *11*, 65. [CrossRef] [PubMed]
100. Karp, J.R.; Hamerski, F.; Silva, V.R. Supported silk fibroin/poly (vinyl alcohol) membrane blends: Structure, properties, and ethanol dehydration by pervaporation. *Polym. Eng. Sci.* **2018**, *58*, 1879–1887. [CrossRef]

101. Selim, A.; Toth, A.J.; Fozer, D.; Szanyi, A.; Mizsey, P. Pervaporative Dehydration of Methanol Using PVA/Nanoclay Mixed Matrix Membranes: Experiments and Modeling. *Membranes* **2020**, *10*, 435. [CrossRef]
102. Baker, R.W. *Membrane Technology and Applications*; McGraw-Hill: New York, NY, USA, 2000.
103. Baker, R.W.; Wijmans, J.; Huang, Y. Permeability, permeance and selectivity: A preferred way of reporting pervaporation performance data. *J. Membr. Sci.* **2010**, *348*, 346–352. [CrossRef]
104. Liu, H.; Jiang, C.; Li, H.; Chen, Z. Preparation of FeBTC/silica aerogels by a co-sol-gel process for organic pollutant adsorption. *Mater. Res. Express* **2019**, *6*, 1250g7. [CrossRef]
105. Dmitrenko, M.; Zolotarev, A.; Liamin, V.; Kuzminova, A.; Mazur, A.; Semenov, K.; Ermakov, S.; Penkova, A. Novel Membranes Based on Hydroxyethyl Cellulose/Sodium Alginate for Pervaporation Dehydration of Isopropanol. *Polymers* **2021**, *13*, 674. [CrossRef]
106. Singh, P.; Baisthakur, P.; Yemul, O.S. Synthesis, characterization and application of crosslinked alginate as green packaging material. *Heliyon* **2020**, *6*, e03026. [CrossRef] [PubMed]
107. Huang, Y.; Zhang, X.; Ma, Z.; Li, W.; Zhou, Y.; Zhou, J.; Zheng, W.; Sun, C. Size, separation, structural order and mass density of molecules packing in water and ice. *Sci. Rep.* **2013**, *3*, 3005. [CrossRef]
108. Mokhtarzadeh, S.; Hakimpour, F.; Sarvari, R.; Agbolaghi, S.; Mansourpanah, Y. Nanocomposite membranes based on sodium alginate/poly (ε-caprolactone)/graphene oxide for methanol, ethanol and isopropanol dehydration via pervaporation. *Polym. Bull.* **2019**, *77*, 3367–3387. [CrossRef]
109. Premakshi, H.; Karidurаganavar, M.Y.; Mitchell, G.R. Crosslinked Nanocomposite Sodium Alginate-Based Membranes with Titanium Dioxide for the Dehydration of Isopropanol by Pervaporation. *Molecules* **2020**, *25*, 1298. [CrossRef]
110. Bhat, S.D.; Aminabhavi, T.M. Novel sodium alginate composite membranes incorporated with SBA-15 molecular sieves for the pervaporation dehydration of aqueous mixtures of isopropanol and 1,4-dioxane at 30 °C. *Microporous Mesoporous Mater.* **2006**, *91*, 206–214. [CrossRef]
111. Karidurаganavar, M.; Kittur, A.; Kulkarni, S.; Ramesh, K. Development of novel pervaporation membranes for the separation of water–isopropanol mixtures using sodium alginate and NaY zeolite. *J. Membr. Sci.* **2004**, *238*, 165–175. [CrossRef]
112. Sajjan, A.M.; Premakshi, H.G.; Karidurаganavar, M.Y. Synthesis and characterization of polyelectrolyte complex membranes for the pervaporation separation of water–isopropanol mixtures using sodium alginate and gelatin. *Polym. Bull.* **2017**, *75*, 851–875. [CrossRef]
113. Choudhari, S.K.; Premakshi, H.G.; Karidurаganavar, M.Y. Development of novel alginate–silica hybrid membranes for pervaporation dehydration of isopropanol. *Polym. Bull.* **2016**, *73*, 743–762. [CrossRef]
114. Rachipudi, P.; Kittur, A.; Sajjan, A.; Kamble, R.; Karidurаganavar, M. Solving the trade-off phenomenon in separation of water–dioxan mixtures by pervaporation through crosslinked sodium–alginate membranes with polystyrene sulfonic acid-co-maleic acid. *Chem. Eng. Sci.* **2013**, *94*, 84–92. [CrossRef]
115. Mali, M.G.; Gokavi, G.S. Sorption and permeation studies for isopropanol + water mixtures using alginate based highly water selective nanocomposite membranes. *J. Polym. Res.* **2012**, *19*, 9976. [CrossRef]
116. Veerapur, R.; Gudasi, K.; Aminabhavi, T. Sodium alginate—magnesium aluminum silicate mixed matrix membranes for pervaporation separation of water–isopropanol mixtures. *Sep. Purif. Technol.* **2008**, *59*, 221–230. [CrossRef]
117. Patil, M.; Veerapur, R.; Patil, S.; Madhusoodana, C.; Aminabhavi, T. Preparation and characterization of filled matrix membranes of sodium alginate incorporated with aluminum-containing mesoporous silica for pervaporation dehydration of alcohols. *Sep. Purif. Technol.* **2007**, *54*, 34–43. [CrossRef]
118. Bhat, S.D.; Aminabhavi, T.M. Novel sodium alginate—Na + MMT hybrid composite membranes for pervaporation dehydration of isopropanol, 1,4-dioxane and tetrahydrofuran. *Sep. Purif. Technol.* **2006**, *51*, 85–94. [CrossRef]